Chemical Geology 269 (2010) 262–277

Contents lists available at ScienceDirect

Chemical Geology

journal homepage: www.elsevier.com/locate/chemgeo

In situ characterization of serpentinites from forearc mantle wedges: Timing of serpentinization and behavior of fluid-mobile elements in subduction zones

Fabien Deschamps [a,*], Stéphane Guillot [a], Marguerite Godard [b], Catherine Chauvel [a], Muriel Andreani [c], Kéiko Hattori [d]

[a] Laboratoire de Géodynamique des Chaînes Alpines, OSUG, Université Grenoble I, 1381 rue de la Piscine, 38400 Grenoble Cedex 09, France
[b] Laboratoire de Géosciences, ISTEEM (UMR 5243), Université Montpellier II, Place E. Bataillon, 34095 Montpellier, France
[c] Laboratoire de Sciences de la Terre (UMR 5570), Université Claude Bernard Lyon I, 2 rue Raphaël Dubois, 69622 Villeurbanne, France
[d] Department of Earth Sciences, University of Ottawa, Ottawa, Ontario, Canada K1N 6N5

ARTICLE INFO

Article history:
Received 13 March 2009
Received in revised form 28 September 2009
Accepted 2 October 2009

Editor: B. Bourdon

Keywords:
High-pressure serpentines
Forearc mantle peridotites
Subduction zones
Hydrated mantle wedge
Fluid-mobile elements recycling

ABSTRACT

The Tso Morari serpentinites in the Ladakh area, northwest Himalaya, originated from the forearc mantle overlying the northward subducting Neo-Tethys lithosphere and the margin of the Indian continent. The serpentinites are characterized by high concentration of fluid-mobile elements (FME: As, Sb, B, Li, and U) compared to ophiolitic or abyssal serpentinites. The Pb isotopic compositions of serpentinites show influence of the subducted Indian continental lithosphere. Trace element concentrations of antigorite determined in situ with Laser Ablation High Resolution Inductively Coupled Mass Spectrometer (LA-HR-ICP-MS) show high contents of FME including Pb, in contrast to the spatially associated iron oxides. Rare earth elements (REE) and compatible elements, such as Sc and Co, remained immobile during the hydration, allowing the identification of the primary minerals (olivine or orthopyroxene) from which serpentine formed. Serpentinized olivine displays higher Sb and As concentrations (up to 1000×PM) than serpentinized orthopyroxenes that are enriched in Pb, Cs and Li (2 to up to 10×PM).

We propose that the observed FME distribution in two types of serpentine reflect the differential incorporation of FME during the downward movement of the serpentinite along the subduction plane. At temperature lower than 400 °C, at shallow depths, olivine is preferentially serpentinized and incorporates elements that are fluid soluble at low temperatures, such as Sb and As. Above 400 °C, orthopyroxene is hydrated and incorporates Pb, Cs, Li and possibly Ba. Boron and U are incorporated in both types of serpentine suggesting that they are released from slabs at temperatures around 300–400 °C. The serpentine acts as a sink for water, but also for FME and transports them to deeper and hotter levels in the mantle, down to the isotherm 600–650 °C where dehydration occurs.

1. Introduction

The serpentinization of mantle peridotites is important in the element transfer from slabs to the mantle during subduction. During the last decade, several geophysical observations documented the occurrence of forearc mantle serpentinites in different locations (e.g., Kamiya and Kobayashi, 2000; Bostock et al., 2002; Brocher et al., 2003; Blakely et al., 2005; Soyer and Unworth, 2006). Serpentinites, which contains up to 13 wt.% of water and are stable up to ~650 °C (down to ~150 km; Wunder et al., 2001), are an important reservoir for chemical recycling in subduction zones (Ulmer and Trommsdorff, 1995). Despite their low trace element concentrations, serpentinites are often enriched in some incompatible and fluid-mobile elements (FME Scambelluri et al., 2001a, 2004; Hattori and Guillot, 2003, 2007; Tenthorey and Hermann, 2004; Savov et al., 2005a). In addition, FME, i.e. elements having high solubility in aqueous fluids (as defined by Leeman, 1996), such as As, Sb, Pb, and B are enriched in arc magmas (Ryan et al., 1995; Noll et al., 1996; Leeman, 1996), leading to a proposal that the deep dehydration of serpentinites is responsible for the geochemical signature of arc magmas (Scambelluri et al., 2001b, 2004; Hattori and Guillot, 2003). Yet, although it is widely accepted that serpentinites contain FME, little data is available on the distribution of trace elements in serpentinites, with the exception of As: Hattori et al. (2005) demonstrated that As is hosted as arsenate (As^{5+}) by antigorite.

In order to better characterize the distribution of trace elements in serpentinites and evaluate the behavior of trace elements during serpentinization, we carried out an in situ trace element study, using a laser (LA)-high resolution (HR)-ICP-MS, of well-characterized serpentinites from the Tso Morari region (Ladakh area, northwest Himalaya; Guillot et al., 2000, 2001). We also conducted the first measurements of

* Corresponding author. Tel.: +33 4 76 51 40 73; fax: +33 4 76 51 40 58.
E-mail address: fabien.deschamps@ujf-grenoble.fr (F. Deschamps).

0009-2541/$ – see front matter © 2009 Elsevier B.V. All rights reserved.
doi:10.1016/j.chemgeo.2009.10.002

Pb isotope compositions to constrain the origin of our samples and the nature of the fluids that hydrated peridotites within the mantle wedge. We then discuss how the primary mineral composition affects the serpentine compositions, and the timing of the incorporation of FME in serpentine during their downward movement along the subduction plane.

2. Geological setting and sample selection

The Tertiary subduction complex of the eastern part of Ladakh area (northwest Himalaya, India) records the intra-oceanic subduction of the Tethyan oceanic lithosphere, the obduction of Nidar and Spontang oceanic arcs, and finally the subduction of the Indian continent margin beneath Eurasia at ~55 Ma (Guillot et al., 2003). Serpentinites along the Zildat normal fault are observed at the boundary between the eclogitic Tso Morari unit and the Indus suture zone; they occur as discontinuous lenses (~100×500 m). Field observations show that serpentinites are intimately associated with retrograded eclogitic lenses of the Tso Morari unit and that serpentinites were exhumed together with eclogites after 50 Ma from a depth of ~100 km (O'Brien et al., 2001, de Sigoyer et al., 2004) to shallow crustal level due to low density and viscosity of serpentinites (Guillot et al., 2001). Previous work documented that the serpentinites associated with the ultra-high pressure (UHP) Tso Morari massif represent the forearc mantle peridotites hydrated by water released from the subducted Indian continental margin (see geological map in Guillot et al., 2001; Hattori and Guillot, 2007).

We selected ten samples that have been well characterized in terms of geological setting, petrology and bulk rock geochemistry (major and trace element, Nd and Sr isotopes; Guillot et al., 2001; Hattori and Guillot, 2007). Among these samples, we selected three representative samples (CH 98A, CH 98B, and CH146) for in situ LA-HR-ICP-MS analyses. All samples have high MgO (36.65–41.82 wt.%), Cr (>2000 ppm) and Ni (>2000 ppm), and low Al_2O_3 (0.37–0.77 wt.%) contents. Al/Si values (0.01–0.021) are lower than the primitive mantle value, indicative of the protolith of refractory mantle peridotite that have undergone high degrees of partial melting (Table 1). CH 98A (Al/Si = 0.017; Mg/Si = 1.471) has a "dunitic" composition with very low Al, whereas CH 146 presents a more "harzburgitic" signature (Al/Si = 0.021; Mg/Si = 1.164). These serpentinites contain mainly antigorite (a high temperature serpentine phase; Evans, 1977; Wunder et al., 2001) and minor magnetite; they are moderately to intensely sheared. Antigorite locally forms blades, with dusty inclusions of magnetite. Presence of minor lizardite (rare veinlets), chrysotile, talc and chlorite was identified by powder X-ray diffraction (Table 1). Presence of the secondary olivine (Mg# = 0.96–0.97; CH 98A and B; Hattori and Guillot, 2007), containing inclusions of antigorite and magnetite, are in agreement with serpentine destabilization at high temperature (>650 °C; Wunder et al., 2001) during their exhumation with associated eclogites (Guillot et al., 2001) or the subduction of the serpentinites to a deep level below the stability field of antigorite.

Table 1
Summary of the main characteristics of Zildat's serpentinites (Tso Morari, Himalaya).

Sample	CH 98A	CH 98B	CH 146
Whole rock chemical compositions (Hattori and Guillot, 2007)			
Mg	24.10	25.22	22.10
Si	16.39	18.77	18.98
Al	0.29	0.20	0.41
Mg/Si	1.47	1.34	1.16
Al/Si	0.02	0.01	0.02
Mineralogy (modified from Guillot et al., 2001; Hattori and Guillot, 2007)			
	Antigorite	Antigorite	Antigorite
	Metamorphic olivine	Metamorphic olivine	Talc
	Minor late chrysotile	Minor late chrysotile	Minor late chrysotile
	(±Lizardite)	(±Lizardite)	Calcite, Mg-calcite (veins)
	Magnetite	Magnetite	Magnetite
	Chromite	Chromite	
	Magnesite		

Microprobe analyses, average (this study)

Number of analysis	Serpentine	Serpentine	Chromite	Serpentine	Magnetite
	n = 6	n = 9	n = 3	n = 15	n = 2
SiO2	43.64	45.64	0.02	43.43	0.16
TiO2	0.01	n.d.	0.04	0.01	0.01
Al2O3	0.52	0.29	8.95	0.7	0.03
Cr2O3	0.04	0.03	55.94	0.19	0.32
MgO	37.51	38.59	7.51	37.615	2.10
FeO	1.22	0.76	23.48	4.33	87.97
MnO	0.04	0.02	0.96	0.09	0.20
NiO	0.10	0.07	0.08	0.34	0.85
CaO	0.16	0.01	0.01	0.13	0.01
Na2O	0.09	0.01	n.d.	0.01	0.01
K2O	0.10	0.01	n.d.	0.01	n.d.
Total	83.43	85.43	96.99	86.85	91.648

Enriched in fluid-mobile elements (As, Sb, and Pb).
High concentrations of Ir-type platinum group elements (PGE).
High XCr in spinel (0.76–0.83).
High 87Sr/86Sr (up to 0.730) and low 143Nd/144Nd.

3. Analytical techniques

Part of each sample was crushed and reduced to powder in an agate ring mill. Whole rock major and trace elements compositions of studied samples are reported by Hattori and Guillot (2007). To avoid possible laboratory biases, additional whole rock trace element data were acquired on the same HR-ICP-MS on which in situ trace element compositions were obtained.

3.1. Whole rock trace element composition

Trace element concentrations (Li, Cd, Co, Ni, Cu, As, Rb, Sr, Y, Zr, Nb, Cs, Ba, Rare Earth Elements (REE), Hf, Ta, Pb, Th, U and W) were determined using a ThermoFinnigan Element2 High Resolution (HR-) ICP-MS at Géosciences Montpellier (University Montpellier 2, France). Most elements were measured in low-resolution mode ($m/\Delta m \sim 400$), except Co, Ni, and Cu that were analyzed in medium resolution mode ($m/\Delta m \sim 4000$) and As, measured in high resolution mode ($m/\Delta m \sim 10000$). The analytical procedure is described in Ionov et al. (1992) and Godard et al. (2000). The method involves dissolution of 100 mg aliquots in an $HF/HClO_4$ mixture and dilution of the solution by a factor ranging from 1000 to 4000 depending on the concentration of the elements. Indium and Bismuth were used as internal standards during ICP-MS measurements. Calibration solution used Merck multi-element standard solutions except for Nb and Ta. To avoid memory effects due to the introduction of concentrated Nb–Ta solutions in the instrument, Nb and Ta concentrations were determined by using, respectively, Zr and Hf as internal standards. This technique is similar to that described in Jochum et al. (1990) for the determination of Nb by spark-source mass spectrometry. The precision and accuracy of the HR-ICP-MS analyses were assessed by measuring as unknowns three rock standards: dunite DTS-1, peridotite JP-1 and serpentinite UBN. Our results show good agreement between obtained values and expected values for these international standards (Govindaraju, 1994; GEOREM http://georem.mpch-mainz.gwdg.de/ — March 12th, 2009), and reproducibility is generally better than 1% at concentrations >1 ppm; it is between 1 and 5% for concentrations of 10–1000 ppb, and between 5 and 10% for concentrations less than 10 ppb. Interference of Ba and LREE on MREE, and those of MREE on HREE and Hf and Ta are corrected following the method described in Ionov et al. (1992). To assess the analytical method, we determined the trace element concentrations of JP-1,

Table 2
Whole rock trace element (HR-ICP-MS) concentrations (in ppm) and 1σ error (ppb) for Zildat's serpentinites (n.d. = not determined).

Sample	CH 98A	1σ error	CH 98B	1σ error	CH 146	1σ error
		ppb		ppb		ppb
Element (ppm)						
Li	n.d.	n.d.	1.36	0.06	11.77	0.71
Co	110	4.67	119	7.20	91.8	4.20
Ni	2216	38.57	2649	87.47	1998	26.66
Cu	4.8	0.16	6.5	0.19	13.8	0.30
As	79.86	0.42	65.17	2.90	6.66	0.61
Rb	0.01	3.74	0.15	4.11	0.35	6.68
Sr	2.52	50.18	7.16	8.44	29.58	267.62
Y	0.220	1.79	0.303	5.31	0.329	3.97
Zr	0.100	2.77	n.d.	n.d.	0.350	6.87
Nb	0.430	41.79	0.578	7.90	0.027	0.26
Cd	0.01	0.004	0.01	0.009	0.02	0.010
Cs	0.026	0.69	0.090	1.17	0.559	2.97
Ba	0.153	10.95	0.722	24.89	5.092	97.51
La	0.0354	0.87	0.0656	0.55	0.0474	0.48
Ce	0.0656	0.95	0.1312	1.97	0.0894	3.46
Pr	0.0065	0.09	0.0135	0.32	0.0116	0.67
Nd	0.0282	0.38	0.0555	0.20	0.0551	4.19
Sm	0.0104	0.72	0.0166	1.09	0.0189	0.93
Eu	0.0400	0.30	0.0058	0.54	0.0144	0.23
Gd	0.0197	1.18	0.0306	0.74	0.0383	1.73
Tb	0.0040	0.13	0.0061	0.35	0.0076	0.15
Dy	0.0344	1.50	0.0474	2.46	0.0622	1.82
Ho	0.0078	0.23	0.0113	0.10	0.0138	0.48
Er	0.0242	0.74	0.0377	1.41	0.0432	2.10
Tm	0.0046	0.12	0.0059	0.36	0.0068	0.18
Yb	0.0354	1.58	0.0408	1.20	0.0500	0.49
Lu	0.0068	0.14	0.0071	0.23	0.0093	0.29
Hf	0.0050	0.17	0.0060	0.25	0.0139	1.28
Ta	0.0005	0.03	0.0015	0.01	0.0013	0.01
W	n.d.	n.d.	2.61	0.18	0.19	0.01
Pb	2.487	15.63	4.688	6.88	3.093	22.45
Th	0.002	0.16	0.02	1.13	0.019	0.29
U	1.279	22.47	1.689	13.29	0.311	4.36

which contains high Ba (9 ppm) and low Eu (3 ppb). The obtained values are 3.00 ppm Eu and 9.83 ppm Ba which is comparable to the accepted value confirming that the analytical method provides reliable data. Detection limits, procedural blanks and values obtained for the rock standards are reported in Appendix A.

3.2. Lead isotopes

At the University of Ottawa, Pb isotope compositions were determined following a conventional procedure using a thermal ionization mass spectrometer (TIMS). Approximately 100 mg of serpentinite powders were rinsed several times in Milli-Q water in an ultrasonic bath before digestion in conc. HNO_3-HBr. Lead was separated and purified using anion resin (BioRad AG1-X8 200–400 mesh) and eluted into a HBr solution. The total procedure blank of 60 to 80 pg was low compared to the amounts of Pb in the samples. Therefore, no blank correction was made to the measured Pb compositions. The isotopic compositions were measured in a static mode with a Thermo-Finnigan Triton multi-collector mass spectrometer at Carleton University in Ottawa. The measured values were corrected using mass fractionation values (<0.1%) obtained from NBS 981.

Because of the extremely low Pb concentrations of serpentinites, we duplicated some of our measurements using a more precise method. The separation and purification of Pb was done at LGCA (Grenoble, France) while the isotopic compositions were measured by MC-ICP-MS at Ecole Normale Supérieure (ENS) of Lyon (France). For Pb elution, we used anionic resin column with HBr (Manhès et al., 1984). Procedural blank was negligible (<50 pg; $n=2$) relative to the amounts of Pb in samples and blank correction was not applied. Pb isotopic ratios were measured on a NU 500 MC-ICP-MS in static multi-collection mode, using the Tl normalization described by White et al. (2000). NBS 981 was run as external standard every two samples, and used to correct Pb isotope ratios by sample-standard bracketing (White et al., 2000; Blichert-Toft et al., 2003) with NBS 981 triple spike thermal ionization mass spectrometer (TIMS) values from Galer and Abouchami (1998).

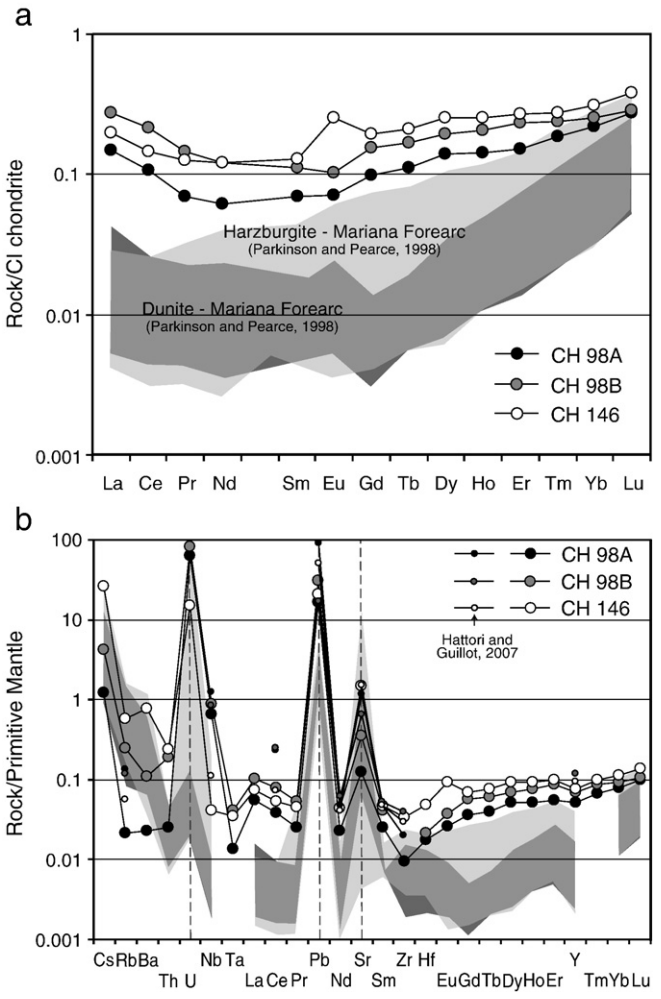

Fig. 1. a.) Chondrite normalized whole rock REE patterns for studied serpentinites from Zildat (Tso Morari-Himalaya). Chondrite normalizing values were taken from McDonough and Sun (1995). Symbols are indicated in insert. b.) Primitive mantle normalized spidergrams. Spidergrams are dominated by relative enrichment in Cs, Sr, U and Pb. Primitive mantle normalizing values were taken from McDonough and Sun (1995). Small symbols are for analyses from Hattori and Guillot (2007). In both diagrams, values from peridotites from the Izu–Bonin–Mariana forearc (Parkinson and Pearce, 1998) are shown in comparison.

No age corrections were applied to our samples because hydrated peridotites cannot be considered as a closed system for U, Th and Pb due to fluid circulation.

3.3. Mineral characterization

A Siemens D5000 X-ray diffractometer at LGIT (Grenoble, France) was used to characterize the mineralogy of bulk rock samples. Major element concentrations of minerals were determined on a Cameca SX 100 electron microprobe at the Laboratory Magma et Volcans (Clermont Ferrand, France). The operating condition was 15 kV accelerating voltage, sample current of 15 nA and counting time of 10 s/element, except for Ni (20 s). Standards used were albite (Na), forsterite (Mg), orthoclase (K), wollastonite (Ca and Si), $MnTiO_3$ (Ti and Mn), Cr_2O_3 (Cr), fayalite (Fe), olivine (Ni), and synthetic Al_2O_3 (Al).

In situ trace element compositions were determined on 150 μm thick polished sections at Géosciences Montpellier (University

Table 3
Pb isotope compositions for Zildat's serpentinites.

Sample	$^{206}Pb/^{204}Pb$	$\pm 2\sigma$	$^{207}Pb/^{204}Pb$	$\pm 2\sigma$	$^{208}Pb/^{204}Pb$	$\pm 2\sigma$
CH 35A (*)	18.1342		15.5984		37.8833	
CH 98A (*)	18.1923		15.6012		37.9291	
CH 98A Bis (*)	18.2317		15.6399		38.0699	
CH 98B	18.2250	±09	15.6399	±09	38.0004	±27
CH 98B Bis	18.2263	±11	15.6221	±12	38.0008	±52
CH 98B (*)	18.2813		15.6439		37.8703	
CH 146	18.2825	±08	15.6257	±09	38.1416	±33
CH 146 (*)	18.2079		15.6073		38.0213	
CH 187	18.2804	±06	15.6302	±12	38.0886	±30
CH 187 (*)	18.2200		15.6142		37.9598	
CH 422	18.6952	±13	15.6748	±12	38.3343	±38
CH 422 Rep	18.5298	±08	15.6604	±10	38.2669	±28
CH 422 (*)	18.5775		15.6400		38.1830	
CH 423	18.4267	±13	15.6530	±15	38.2418	±38
CH 423 (*)	18.3760		15.6178		38.1331	
CH 430	18.8509	±12	15.7136	±11	38.8257	±30
CH 432	18.6613	±29	15.6698	±25	38.3374	±68
CH 433	18.7814	±13	15.7076	±13	38.7899	±45
CH 433 (*)	18.8823		15.7338		38.8894	
MC-ICP-MS standards						
NBS 981						
Galer and Abouchami, 1998	16.9405		15.4963		36.7219	
Average ($n=11$)	16.9395	±330	15.4892	±174	36.6968	±224
Biais (ppm)	60		459		683	

Errors are given at the 2σ level. Samples annotated with an (*) were determined using a TIMS at the University of Ottawa whereas others were determined on a MC-ICP-MS at ENS-Lyon.

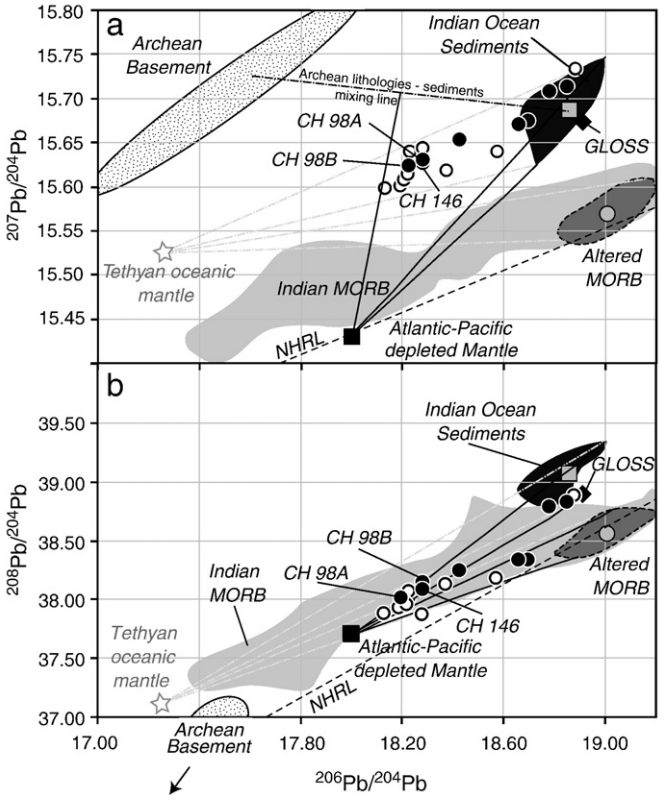

Fig. 2. $^{207}Pb/^{204}Pb$ (a) and $^{208}Pb/^{204}Pb$ (b) vs. $^{206}Pb/^{204}Pb$ diagrams for Zildat serpentinites (black and white circle are data from TIMS analysis (Ottawa) and black circle are data from MC-ICP-MS analysis (Grenoble-Lyon); see Analytical methods); no age correction due to the open system. Published data by Mahoney et al. (1998, 2002) for Indian MORB and altered Pacific oceanic crust (average reported with a grey circle; Mahoney et al., 1998) are shown. Present day depleted mantle value for Atlantic and Pacific Ocean (black square; Rehkämper and Hofmann, 1997) and Northern Hemisphere Reference Line (Hart, 1984) are reported for comparison. Field and average composition (grey square) for Indian Ocean sediments are from Ben Othman et al. (1989), and average composition of global subducting sediments (GLOSS; black diamond) is from Plank and Langmuir (1998). Fields for Indian Archean basement are compiled from Russell et al. (1996) and Chakrabarti and Basu (2006). Lherzolite lens from Kohistan area representing pre arc Indian lithospheric mantle are from Dhuime et al. (2007). Mixing lines between depleted mantle (black curve) or pre Tethyan oceanic mantle (light grey and dotted curve) and altered MORB and Indian Ocean sediments are represented. Moreover, mixing (black curve) between depleted mantle and mixing line (dark and dotted line) between Archean lithologies and Indian Ocean sediments is also shown. Compositions of the end-members used for the calculations are the following: (a) Lherzolite lens: Pb = 2.53 ppm, $^{206}Pb/^{204}Pb = 17.26$, $^{207}Pb/^{204}Pb = 15.523$ and $^{208}Pb/^{204}Pb = 37.104$ (Dhuime et al., 2007); (b) Depeleted mantle (Atlantic and Pacific Ocean): Pb = 0.0489 ppm, $^{206}Pb/^{204}Pb = 18$, $^{207}Pb/^{204}Pb = 15.43$ and $^{208}Pb/^{204}Pb = 37.7$ (Rehkämper and Hofmann, 1997); (c) less radiogenic Indian Ocean sediments: Pb = 13.06 ppm, $^{206}Pb/^{204}Pb = 18.738$, $^{207}Pb/^{204}Pb = 15.624$ and $^{208}Pb/^{204}Pb = 38.867$; (d) more radiogenic Indian Ocean sediments: Pb = 22.92 ppm, $^{206}Pb/^{204}Pb = 18.985$, $^{207}Pb/^{204}Pb = 15.745$ and $^{208}Pb/^{204}Pb = 39.26$ (Ben Othman et al., 1989); (e) less radiogenic altered MORB sample: Pb = 0.1211 ppm, $^{206}Pb/^{204}Pb = 18.928$, $^{207}Pb/^{204}Pb = 15.545$ and $^{208}Pb/^{204}Pb = 38.398$; (f) more radiogenic altered MORB sample: Pb = 0.7713 ppm, $^{206}Pb/^{204}Pb = 19.187$, $^{207}Pb/^{204}Pb = 15.596$ and $^{208}Pb/^{204}Pb = 38.721$ (Mahoney et al., 1998).

Montpellier 2, France) with a ThermoFinnigan Element 2 HR-ICP-MS using a single collector double-focusing sector field Element XR (eXtended Range) coupled with laser ablation (LA) system, a Geolas (Microlas) automated platform housing a 193 nm Compex 102 laser from LambdaPhysik. Analyses were conducted using a modified ablation cell of ca. 30 cm^3, which resulted in a shorter washout time and an improved sensitivity compared to the initial larger ablation cell. Ablation was conducted in a helium atmosphere, which enhances sensitivity and reduces inter-element fractionation (Gunther and Heinrich, 1999). The helium gas and particles from a sample were then mixed with argon gas before entering the plasma. Signals were acquired in Time Resolved Acquisition, devoting 2 mn for the blank and 1 mn for the measurement itself. The laser was fired using an energy density of 15 J cm^{-2} at a frequency of 7 Hz and the beam size on the surface of samples are 77 μm for sample CH 98A, and 122 μm for samples CH 98B and CH 146. The size was larger than the grain size, but it was necessary to get good accuracy on our results. This resulted in a sensitivity of ~500 cps/ppm for B, ~2000 cps/ppm for Li, Ni, Ti, Zn, As and Cr, and ~18,000 cps/ppm for the other analyzed elements based on measurements on the NIST 612 certified reference material. Oxide formation was monitored by measuring the ThO/Th ratio, and was below 0.7%. ^{29}Si was used as internal standard. Concentrations were calibrated against the NIST 612 rhyolitic glass using the values given in Pearce et al. (1997). Data were subsequently reduced using the GLITTER software (Van Achterberg et al., 2001) using the linear fit to ratio method. This typically resulted in a 5 to 10% precision (1sigma) for most analyses evaluated by repeated analyses of reference basalt BIR 1-G (Supplementary dataset — Appendix B; preferred values from Jochum et al., 2005; Jochum and Stoll, 2008). Detection limits were below 0.05 ppm for all elements except Li, B, Ti, Cr, Ni, Zn and As (between 0.06 and 3 ppm). Note that we did a logical test ((Values − 2σ error)>detection limit) to eliminate values too close from the detection limit.

Due to the thickness of our sections (~150 μm), the small grain size of serpentine, the thinness of individual crystals serpentine and the intense deformation of minerals, we were not able to distinguish the texture (mesh or bastite) of analyzed grains. Moreover, due to the large beam size (up to 122 μm) it used to get a good signal, it was impossible to distinguish polymorphs of serpentine (mostly antigorite, but also minor lizardite and/or chrysotile). Antigorite commonly forms blades with numerous dusty inclusions of magnetite and other minor secondary phases (chlorite, calcite, chrysotile and lizardite). To minimize the contribution of other phases, we analyzed the clear areas with texture and characteristic blade shape of antigorite, in the limit of apparatus optical resolution. Despite low concentrations of most trace elements and the

Table 4
Trace element analyses (HR-LA-ICP-MS) of serpentine minerals after olivine or pyroxene, and iron oxides from Zildat serpentinites.

Sample	CH 98A	CH 98A	CH 98A	CH 98A	CH 98A	CH 98A	CH 98B	CH 98B	CH 98B
	# 1	# 2	# 3	# 4	# 5	# 6	# 7	# 8	# 9
Spot size	77 μm	77 μm	77 μm	77 μm	77 μm	77 μm	122 μm	122 μm	122 μm
Minerals	Serpentine	Serpentine	Serpentine	Serpentine	Serpentine	Serpentine	Serpentine	Serpentine	Serpentine
Group	1	1	1	1	1	1	1	1	1
Primary mineral	Olivine	Olivine	Olivine	Olivine	Olivine	Olivine	Olivine	Olivine	Olivine
Li	b.d.l.	b.d.l.	0.21	0.31	0.78	0.48	0.36	0.18	b.d.l.
B	85.0	73.6	54.1	67.3	83.8	91.2	139.8	89.6	142.4
Si (%)	41.5	43.1	43.4	44.0	44.8	45.1	45.6	41.8	45.6
Ca	b.d.l.	b.d.l.	b.d.l.	47.0	156.0	33.8	705.8	74.6	39.4
Sc	4.0	3.4	3.4	2.6	5.5	5.4	2.2	2.0	2.3
Ti	19.7	15.1	15.4	14.4	25.1	26.9	11.7	7.4	11.5
V	12.3	10.9	9.7	8.0	31.4	9.7	4.9	2.7	5.0
Cr	1756	838.0	391.0	312.6	1510	888.0	774.7	195.7	782.7
Co	30.0	29.1	42.8	39.9	35.3	n.d.	64.2	20.0	32.5
Ni	733	669	1158	1145	985	1141	1931	420	1253
Cu	3.2	0.5	3.1	1.6	6.5	4.3	16.2	2.4	9.4
Zn	12	12	16	14	13	9	15	11	12
As	26.17	23.40	18.49	20.97	25.68	32.53	54.63	19.40	54.92
Rb	b.d.l.	b.d.l.	0.029	0.040	0.029	0.045	0.069	b.d.l.	0.029
Sr	0.197	0.039	0.247	26.140	0.116	0.115	2.445	0.652	0.137
Y	0.236	0.246	0.096	0.119	0.196	0.191	0.247	0.239	0.343
Zr	b.d.l.	b.d.l.	b.d.l.	0.081	0.071	0.324	0.086	0.075	0.110
Nb	0.255	0.219	0.124	0.182	0.322	0.276	0.379	0.299	0.290
Sb	9.45	9.25	4.16	6.02	8.01	9.33	12.12	11.45	18.37
Cs	0.043	0.011	0.016	0.006	0.010	b.d.l.	0.049	b.d.l.	0.021
Ba	0.083	0.035	0.101	0.014	0.089	0.084	0.933	0.040	0.035
La	0.0441	0.0293	0.0103	0.0174	0.0352	0.0216	0.0392	0.0457	0.0473
Ce	0.0643	0.0494	0.0356	0.0369	0.0605	0.053	0.0685	0.0874	0.1141
Pr	b.d.l.	0.0072	b.d.l.	b.d.l.	0.0063	n.d.	0.0085	0.0062	0.0112
Nd	0.0333	b.d.l.	b.d.l.	0.0243	b.d.l.	b.d.l.	0.0208	0.0330	0.0434
Sm	b.d.l.	b.d.l.	b.d.l.	0.0069	0.0146	b.d.l.	b.d.l.	0.0184	0.0185
Eu	0.0096	n.d.	0.0060	b.d.l.	b.d.l.	0.0101	b.d.l.	0.0046	0.0071
Gd	n.d.	n.d.	b.d.l.	b.d.l.	b.d.l.	b.d.l.	0.0106	0.0228	0.0391
Tb	b.d.l.	b.d.l.	b.d.l.	b.d.l.	b.d.l.	b.d.l.	0.0038	0.0045	0.0083
Dy	0.0252	0.0314	0.0156	b.d.l.	0.0334	0.0189	0.0352	0.0287	0.0502
Ho	0.0104	0.0091	0.0020	0.0015	0.0075	0.0072	0.0087	0.0055	0.0123
Er	0.0193	0.0126	b.d.l.	0.0067	0.0135	0.0120	0.0176	0.0251	0.0357
Tm	0.0054	0.0052	0.032	b.d.l.	0.0033	0.0026	0.0050	b.d.l.	0.0052
Yb	0.0387	0.0376	b.d.l.	0.0137	0.0384	0.0273	0.0237	0.0136	0.0255
Lu	n.d.	n.d.	0.0106	0.0051	0.0054	0.0038	0.0045	0.0024	0.0028
Hf	b.d.l.	b.d.l.	b.d.l.	0.0186	0.2810	0.1330	0.0015	b.d.l.	b.d.l.
Ta	b.d.l.	b.d.l.	b.d.l.	0.0048	b.d.l.	b.d.l.	0.0004	0.0010	0.0016
Pb	0.166	0.051	0.276	0.125	0.518	0.158	0.461	0.389	0.403
Th	0.004	0.001	0.006	0.025	n.d.	0.007	b.d.l.	0.002	0.004
U	0.340	0.145	0.527	0.370	0.700	0.585	0.600	0.057	0.887

All elements are in ppm, except Si in wt.% (n.d. = not determined; b.d.l. = below detection limit).

small grain size (less than 100 μm) of serpentine minerals, LA-HR-ICP-MS analyses yield a good reproducibility (Table 4).

4. Results

4.1. Whole rock trace element compositions

Results of whole rock trace element analyses for Tso Morari serpentinites are reported in Table 2. Rare earth elements (REE) normalized to C1-chondrite values (McDonough and Sun, 1995) show a concave upward pattern with slight enrichment in light REE (LREE) compared to middle REE ($1.57<La_N/Sm_N<2.46$: N: normalized to CI-chondrite), and a stronger depletion in middle REE relative to heavy REE (HREE; $0.45<Gd_N/Yb_N<0.62$) (Fig. 1a). All samples are LREE depleted relative to HREE ($La_N/Yb_N\approx0.65$) except for sample CH 98B ($La_N/Yb_N\approx1.1$). Samples CH 98A and CH 98B show a slight negative Eu anomaly ($Eu/Eu^*\approx0.8$) whereas CH 146 is characterized by high Eu content ($Eu/Eu^*\approx1.6$). Extended trace element patterns normalized to primitive mantle (PM) (Fig. 1b) are characterized by the enrichments in Th and alkali and alkali–earth elements, such as Cs, Rb, Ba and Sr, relative to neighboring REE as well as by strong U and Pb enrichments, up to ten times PM values of McDonough and Sun (1995). These spiked patterns are similar to those observed in forearc (Savov et al., 2005a,b) and ophiolitic serpentinites (Li and Lee, 2006), although we note that the Tso Morari serpentinites are less REE depleted than Mariana forearc serpentinites (Fig. 1). Dunitic samples CH 98A and CH 98B show a significant enrichment in Nb with the weight ratios of Nb/Ta ranging from 385 to 860, whereas harzburgitic CH 146 show a moderate enrichment of Nb with the ratios of ≈21, which is significantly higher than 17.8 for the ratio of primitive mantle (McDonough and Sun, 1995). They do not show a strong fractionation between Zr and Hf ($20<Zr/Hf<25.18$; PM = 37.10, McDonough and Sun, 1995). Finally, dunitic samples CH 98A and CH 98B are enriched in As (>65 ppm), Ni (2300–2700 ppm), Co (110–120 ppm) and W (2.5 ppm) relative to harburgitic sample CH 146 (As = 7 ppm; Ni = 2000 ppm; Co = 90 ppm; W = 0.2 ppm). In contrast, CH146 has higher Li contents (12 ppm) than CH 98A and CH 98B (1.4 ppm).

Overall, the new trace element data are consistent with the previous analyses of the same samples within the analytical uncertainty (Hattori and Guillot, 2003, 2007), although the new values are

CH 98B	CH 98B	CH 98B	CH 98B	SCH 98B	CH 98B	CH 98B	CH 146	CH 146	CH 146
# 10	# 11	# 12	# 13	# 14	# 15	# 16	# 17	# 18	# 19
122 μm	122 μm	122 μm	122 μm	122 μm	122 μm	122 μm	122 μm	122 μm	122 μm
Serpentine	Serpentine	Serpentine	Serpentine	Serpentine	Serpentine	Serpentine	Serpentine	Serpentine	Serpentine
1	1	1	1	2	2	2	2	2	2
Olivine	Olivine	Olivine	Olivine	Pyroxene	Pyroxene	Pyroxene	Pyroxene	Pyroxene	Pyroxene
0.11	0.11	0.13	0.24	2.79	3.70	3.09	7.76	14.76	7.71
134.6	56.4	124.7	188.2	121.4	72.4	102.6	71.6	97.2	94.3
41.8	41.8	45.6	45.6	45.6	41.8	45.6	40.7	44.9	44.5
35.8	19.0	27.4	44.9	755.7	56.5	67.4	554.9	1265	614.9
2.0	1.6	2.1	2.5	9.3	13.9	8.0	8.0	8.4	9.5
10.2	5.6	10.6	11.9	29.3	14.9	11.3	111.1	96.1	116.7
3.3	1.7	3.4	4.4	0.5	0.3	0.9	32.0	29.9	36.1
445.7	107.8	461.5	710.2	82.2	161.9	134.6	861.9	3212	748.0
22.1	21.1	21.7	46.7	150.3	158.4	131.3	109.7	183.1	120.6
709	436	679	2180	3002	2728	2831	1052	991	631
5.8	1.8	5.5	18.8	10.7	1.4	5.7	10.4	4.9	3.5
11	13	13	10	40	48	37	25	24	25
39.27	11.08	36.00	75.88	22.73	3.97	19.04	6.54	6.04	7.04
0.034	0.032	0.047	n.d.	0.094	0.043	0.037	0.078	0.092	0.063
0.129	0.024	0.103	0.256	2.100	0.178	0.225	1.830	3.840	1.980
0.354	0.139	0.260	0.312	0.187	0.141	0.112	0.187	0.471	0.207
0.108	0.065	0.083	0.092	0.094	0.660	0.054	0.709	0.387	0.241
0.221	0.261	0.295	0.355	0.951	0.020	0.315	0.006	0.020	0.013
15.03	5.64	15.71	20.49	0.71	0.40	1.13	0.46	0.64	0.50
0.007	b.d.l.	0.010	0.033	0.065	0.068	0.044	0.091	0.099	0.080
0.064	0.031	0.059	0.083	0.135	0.411	0.098	1.500	3.830	1.520
0.0973	0.0183	0.0441	0.0523	0.0189	0.0133	0.0095	b.d.l.	0.0086	b.d.l.
0.1129	0.0428	0.0925	0.0918	0.0369	0.0162	n.d.	n.d.	0.0196	0.0410
0.0121	0.0057	0.0088	0.0104	0.0039	0.0021	0.0093	b.d.l.	0.0019	0.0019
0.0501	0.0122	0.0470	0.0694	0.0202	n.d.	b.d.l.	0.0072	0.0184	0.0416
0.0408	n.d.	0.0109	0.0238	n.d.	b.d.l.	n.d.	b.d.l.	0.0182	b.d.l.
0.0067	0.0055	0.0061	n.d.	0.0028	b.d.l.	0.0029	0.0073	0.0099	0.0105
0.0405	0.0156	0.0286	0.0167	0.0085	0.0141	b.d.l.	b.d.l.	0.0404	0.0190
0.0065	0.0030	0.0047	0.0059	0.0020	n.d.	n.d.	0.0021	0.0083	0.0047
0.0617	0.0210	0.0364	0.0531	0.0138	0.0191	0.0131	0.0327	0.0714	0.0337
0.0102	0.0032	0.0099	0.0110	0.0075	0.0102	0.0041	0.0076	0.0168	0.0083
0.0341	0.0122	0.0301	0.0239	0.0249	0.0312	0.0218	0.0316	0.0543	0.0308
0.0066	0.0026	0.0035	0.0038	0.0094	0.0102	0.0080	0.0058	0.0120	0.0072
0.0408	0.0128	0.0130	0.0320	0.1057	0.1582	0.0597	0.0477	0.0790	0.0531
0.0040	0.0019	0.0030	0.0031	0.0167	0.0389	0.0181	0.0065	0.0180	0.0072
0.0038	0.0016	0.0072	0.0035	0.0059	0.0018	n.d.	0.0123	0.0241	0.0153
0.0010	0.0015	b.d.l.	b.d.l.	b.d.l.	b.d.l.	b.d.l.	b.d.l.	b.d.l.	b.d.l.
0.294	0.389	0.552	1.070	0.600	0.475	0.584	0.345	0.501	5.620
0.003	0.003	0.002	0.005	0.095	0.199	b.d.l.	0.004	0.001	0.002
0.498	0.021	0.305	0.714	0.314	0.051	0.235	0.004	0.113	0.002

systematically lower for Ce, Sr, Y, Nb and Pb. Nevertheless, our results confirm the high concentrations of FME pointed out by Hattori and Guillot (2003), notably for As except in sample CH 98A (80 ppm — this study; 275 ppm — Hattori and Guillot, 2007). The sample was noted with a strong X-ray absorption spectrum or As K-edge compared to other samples (Hattori et al., 2005). Therefore, the difference in As concentration in CH 98A may be related to the different analytical methods used to determine this element or to its uneven distribution in the samples (e.g., high concentration in microphases).

To summarize the results from this study and those published by Hattori and Guillot (2003, 2007), dunitic samples CH 98A and CH 98B display high Mg/Si ratios and are enriched in As (65–80 ppm), Sb (10 – 12 ppm), U (1.28–1.69 ppm), and Nb (0.43–0.58 ppm) compared to "harzburgitic" sample CH 146 (7, 0.69, 0.311, and 0.027 ppm, respectively). On the other hand, CH 146 presents high enrichment in Sr (30 ppm), Li (12 ppm), Ba (5 ppm), and Cs (0.6 ppm). Some FME such as As, Sb, and U, which are soluble at low temperatures appear to be preferentially incorporated in serpentinites with an olivine-rich protolith. On the other hand, less incompatible FME, such as Li, Ba or Sr, are enriched in serpentinites originated from a harzburgitic protolith.

4.2. Lead isotopic compositions

Isotopic compositions of Pb are reported in Table 3 and plotted in Fig. 2. The ratios of $^{206}Pb/^{204}Pb$ vary from 18.13 to 18.88, those of $^{207}Pb/^{204}Pb$ from 15.60 to 15.73, and those of $^{208}Pb/^{204}Pb$ from 37.87 to 38.89. All samples define a linear trend between a depleted mantle source and a radiogenic "sedimentary-type" component. The high values are close to the field defined by Indian Ocean sediments (Ben Othman et al., 1989).

4.3. Mineral trace element compositions

X-ray diffraction patterns suggest that samples CH 98A and CH 98B predominantly consist of antigorite ± lizardite, whereas sample CH 146 contains mainly antigorite + talc ± chrysotile. Serpentine minerals from Tso Morari serpentinites are slightly enriched in MgO (33.85–38.59 wt.%; Table 1), SiO_2 (42.64–45.64 wt.%), and strongly enriched in FeO(t) (up to ≈4 wt.%) compared to stoichiometric composition or serpentines minerals in abyssal peridotites (Moll et al., 2007). The high Si concentration of our antigorite is most likely attributed to the

Table 4 (*continued*)

Sample	CH 146	CH 146	CH 146	CH 146	CH 146	CH 146	CH 146	CH 98B	CH 98B
	# 20	# 21	# 22	# 23	# 24	# 25	# 26	# 27	# 28
Spot size	122 μm	122 μm	122 μm	122 μm	122 μm	122 μm	122 μm	122 μm	122 μm
Minerals	Serpentine	Serpentine	Serpentine	Serpentine	Serpentine	Serpentine	Serpentine	Magnetite *with minor carbonates*	Magnetite
Group	2	2	2	2	2	2	2		
Primary mineral	Pyroxene	Pyroxene	Pyroxene	Pyroxene	Pyroxene	Pyroxene	Pyroxene		
Li	8.67	15.14	16.75	17.85	12.91	12.97	9.25	b.d.l.	b.d.l.
B	89.6	96.1	58.1	73.2	58.3	60.7	48.8	0.3	0.1
Si (%)	43.1	43.7	43.9	43.4	41.4	41.6	43.2	0.03	0.03
Ca	751.1	825.7	840.1	1043	689.5	896.5	20846	14.9	1.5
Sc	9.8	7.7	11.3	10.0	10.1	8.7	3.0	0.1	0.005
Ti	112.8	85.7	110.7	126.9	112.0	112.1	32.4	12.5	0.8
V	36.4	30.9	45.2	44.5	38.5	38.1	12.6	23.2	1.7
Cr	876.9	1572	2312	3658	1384	1742	2007	11724	573.8
Co	129.6	160.6	223.0	200.4	159.0	124.6	62.4	37.5	3.4
Ni	606	513	583	539	404	328	159	260	61
Cu	3.9	4.3	5.5	5.1	14.3	40.0	8.5	0.2	0.03
Zn	23	23	35	38	35	33	34	122	10
As	7.13	5.28	8.74	11.89	8.53	9.76	4.34	0.59	0.33
Rb	0.071	0.083	b.d.l.	0.107	0.113	0.078	0.085	0.076	0.002
Sr	2.080	3.480	4.230	4.290	2.750	3.630	28.480	0.025	0.004
Y	0.226	0.355	0.433	0.740	0.317	0.235	0.185	0.007	0.0004
Zr	0.257	0.693	0.401	0.366	0.288	0.335	0.334	0.015	0.001
Nb	0.012	0.013	b.d.l.	b.d.l.	b.d.l.	b.d.l.	b.d.l.	0.014	0.001
Sb	0.54	0.52	0.64	0.90	0.71	0.79	0.17	0.02	0.01
Cs	0.091	0.084	0.090	0.155	0.164	0.138	0.194	0.005	0.0003
Ba	1.540	3.590	4.240	3.610	2.680	3.910	2.110	0.020	0.003
La	0.0039	0.0087	0.0052	0.0326	b.d.l.	b.d.l.	0.0251	0.0010	0.0001
Ce	0.0044	0.0647	b.d.l.	0.0239	b.d.l.	0.0240	0.0251	0.0043	n.d.
Pr	0.0015	0.0078	b.d.l.	0.0133	b.d.l.	b.d.l.	b.d.l.	0.0001	0.0000
Nd	0.0079	0.0084	b.d.l.	0.0630	b.d.l.	b.d.l.	b.d.l.	n.d.	n.d.
Sm	n.d.	b.d.l.	b.d.l.	b.d.l.	b.d.l.	b.d.l.	b.d.l.	0.0019	b.d.l.
Eu	0.0047	0.0095	b.d.l.	b.d.l.	b.d.l.	0.0243	b.d.l.	0.0033	b.d.l.
Gd	0.0209	0.0230	0.1210	0.0960	b.d.l.	b.d.l.	b.d.l.	0.0019	b.d.l.
Tb	0.0029	0.0116	b.d.l.	0.0090	b.d.l.	b.d.l.	b.d.l.	b.d.l.	0.00002
Dy	0.0360	0.0534	0.0600	0.1040	0.0550	0.0445	0.0233	0.0011	0.00004
Ho	0.0131	0.0148	n.d.	0.0270	0.0093	0.0098	0.0119	0.0002	0.00003
Er	0.0400	0.0407	0.0700	0.0900	0.0438	0.0291	0.0297	0.0020	0.0001
Tm	0.0078	0.0095	0.0153	b.d.l.	b.d.l.	0.0082	b.d.l.	n.d.	0.00002
Yb	n.d.	0.0611	0.0870	0.1160	0.0740	0.0430	0.0340	0.0019	b.d.l.
Lu	0.0082	0.0113	0.0171	0.0254	0.0167	b.d.l.	b.d.l.	0.0003	0.00002
Hf	0.0159	0.0276	b.d.l.	b.d.l.	0.0344	b.d.l.	0.0195	0.0010	0.0034
Ta	b.d.l.	b.d.l.	b.d.l.	b.d.l.	b.d.l.	b.d.l.	b.d.l.	0.0004	0.00004
Pb	0.302	0.343	0.500	0.510	0.304	0.253	0.316	0.156	0.010
Th	0.001	b.d.l.	b.d.l.	b.d.l.	b.d.l.	b.d.l.	b.d.l.	0.005	0.001
U	0.001	0.004	b.d.l.	b.d.l.	0.005	0.004	0.078	0.003	0.001

partial dehydration under high pressure (*P*) and temperature (*T*) as Wunder et al. (2001) demonstrated an increase in Si during the partial dehydration of antigorite at high *P* and *T*.

Trace element compositions for serpentine minerals and Fe-oxides are reported in Table 4. Despite low concentrations of most trace elements and the small grain size (less than 100 μm) of serpentine minerals, LA-HR-ICP-MS analyses yield a good reproducibility (Table 4). REE normalized to C1-chondrite show two different patterns (group 1 and 2; Fig. 3), although all have similar major element compositions. Serpentine minerals from group 1 display flat REE patterns ($La/Yb_{N\text{-average}} = 1.17$) whereas serpentine minerals from group 2 show high HREE ($La/Yb_{N\text{-average}} = 0.149$). The groups 1 and 2 patterns resemble those of olivine and orthopyroxene, respectively, in peridotite xenoliths from southeastern British Columbia (Sun and Kerrich, 1995; Fig. 3a, b).

Groups 1 and 2 serpentines show similar trace element patterns on PM-normalized spidergrams (Fig. 4a, b). As already noticed for the whole rocks, both groups of serpentine display positive anomalies in U, Pb and Cs. Some analyses (e.g. # 4 and # 26; Table 4) show high Sr and Ca suggesting the presence of minor carbonate grains in the serpentine. Group 1 serpentines contain high concentrations of Nb relative to Ta (Nb/Ta ranging from 37 to 1024; Nb 0.006–0.95 ppm), and display a variation in Zr/Hf ratios that is not correlated with any other parameters (Fig. 4). Group 2 serpentines are characterized by high concentrations of Sc, Co, V, Zn, Cr, and Ti (Fig. 5).

Fluid-mobile elements such as B (49–188.2 ppm), As (4–76 ppm), Sb (0.2–20.5 ppm), Li (0.1–17.9 ppm) and U (up to 0.9 ppm) are strongly enriched in both groups of serpentine (0.1 up to 1000 times PM values). The high FME content of serpentine minerals is consistent with whole rock analyses (this study, Hattori and Guillot, 2003, 2007). The in situ analyses reveal heterogeneous distribution of FME, and the enrichment appears related to primary mineral (Fig. 6) as already mentioned for the REE. Group 1 serpentines display higher concentrations of Sb (4.2–20.5 ppm in group 1; 0.40–1.13 ppm in group 2), As (11.1–75.9 ppm in group 1; 3.97–22.7 ppm in group 2), U and B than group 2. On the other hand, group 2 serpentines are enriched in Pb, Cs, Li, Ba and Sr (Table 4).

Iron oxides contain very low concentrations of REE and all lithophile elements, close to the detection limits, but high Pb contents

(Table 4). The concentrations of As (0.33–0.59 ppm) and Sb (0.01–0.02 ppm) are higher than the PM values, while B and U are lower than the PM values. Lithium was not detected.

5. Discussion

5.1. Nature of peridotite protoliths and origin of hydrating fluids

To our knowledge, no Pb isotopic compositions have been reported yet on samples from the serpentinized mantle wedge. The Tso Morari serpentinites show isotopic characteristics similar to island arc magmas in the area, reflecting interaction with fluids of sedimentary origin, in agreement with models of Guillot et al. (2001) and Mahéo et al. (2004). The Pb isotope compositions form a linear trend in the $^{208}Pb/^{204}Pb$ vs. $^{206}Pb/^{204}Pb$ diagram (Fig. 2) that can be attributed to three component mixing between a depleted mantle component (Rehkämper and Hofmann, 1997) and two radiogenic components released from subducted slab: sediments similar to present-day Indian Ocean sediments (Ben Othman et al., 1989), and altered MORB (Mahoney et al., 1998). However, these three sources do not account for the radiogenic $^{207}Pb/^{204}Pb$ ratios of our samples (Fig. 2a). A study by Dhuime et al. (2007) suggested that $^{207}Pb/^{204}Pb$ in the Indian pre-arc lithospheric mantle (Neo-Tethys lithospheric mantle) was more radiogenic than the average depleted mantle values (Rehkämper and Hofmann, 1997). This suggestion is based on the analysis of a single lherzolite lens in the Jijal ultramafic–mafic complex of the Kohistan complex (N Pakistan). If we assume that the metasomatized mantle wedge is essentially made of radiogenic $^{207}Pb/^{204}Pb$ Neo-Tethyan lithospheric mantle having a composition similar to that of the Jijal lherzolite, our data plot along sediments and crustal mixing lines. The proposed interpretation is warranted because (1) the closure of the Neo-Tethys in the Ladakh–Zanskar area was suggested by Mahéo et al. (2004), and because (2) a forearc mantle wedge origin for the studied serpentinites was suggested by Guillot et al. (2001). Calculated mixing curves using the Jijal lherzolite as the depleted end-member show a sedimentary input between 16 and 28% for most mafic samples. However, considering the unusually high Pb concentration of the Jijal lherzolite (2.53 ppm; Dhuime et al., 2007), further work is required to confirm that such a rock represents the depleted mantle component.

Another possible source of radiogenic Pb is Archean continental rocks. On the basis of Nd and Sr isotopes, Guillot et al. (2001) and Hattori and Guillot (2007) suggested that serpentinites incorporated FME that were discharged from sediments derived from Archean rocks. Indeed, the subducted northern margin of the Indian continent was covered by shallow water sediments formed from Archean granitic rocks. Moreover, Miller et al. (1999) suggested from $^{207}Pb/^{204}Pb$ ratios that recycled continent-derived material contributed to potassic and ultrapotassic volcanic rocks in the SW Tibet. The Pb isotopic field for the Indian Archean basement (Russell et al., 1996; Chakrabarti and Basu, 2006) is very unradiogenic in $^{208}Pb/^{204}Pb$ but very radiogenic in $^{207}Pb/^{204}Pb$ (Fig. 2a). Concentrations of Pb in granitic rocks and sediments are high compared to those of Pb in mantle peridotites and it is likely that Pb could overwhelm the isotopic signature of the protolith.

Serpentinites at the base of the mantle wedge are a temporary reservoir of water and FME coming from the slab and they transfer geochemical signatures from slab to mantle wedge, and later to arc magmas, during their downward movement as proposed by Hattori and Guillot (2003). The Pb isotopic compositions of the Tso Morari serpentinites suggest that Pb was derived from a forearc mantle lithosphere, which was contaminated, probably in a forearc environment, by fluids sampling, to different extents, different components of slab. The two main sources of slab contaminant are the Indian oceanic sediments and sediments formed from an Archean basement, both sources being probably mixed on the Indian margin before obduction.

5.2. Preservation of the trace element signature of primary minerals during serpentinization

The studied serpentinites result from the hydration (up to 12 wt.% H_2O) of dunitic to harzburgitic peridotites. They include serpentine minerals + magnetite ± talc (± brucite). Geochemical studies of serpentinite have shown that, in spite of the mineralogical changes in peridotites due to serpentinization, major elements are not significantly remobilized at the hand-sample scale with the exception of Ca (Miyashiro et al., 1969; Coleman and Keith, 1971; Komor et al., 1985; Mével, 2003). Whole rock studies of serpentinized abyssal peridotites also show little modification of their trace element composition during the early stages of serpentinization (rock-dominated serpentinization), except for some FME such as U or Sr (e.g. Niu, 2004; Paulick et al., 2006). Therefore, whole rock major and trace element compositions are helpful to determine the nature of the protolith of serpentinites in subduction zones (Chalot-Prat et al., 2003; Hattori and Guillot, 2007). In contrast, little is known about the redistribution of trace elements between secondary phases during serpentinization processes (Menzies et al., 1993; Mével, 2003).

Because our samples underwent significant deformation during exhumation, it was not possible every time to distinguish primary minerals based on textures, such as the pseudomorphic mesh and hourglass texture of olivine or bastite textures of orthopyroxene (Wicks and Whittaker, 1977; Dungan, 1979). Therefore 2 groups of serpentine minerals were distinguished on the basis of their chemical compositions (Section 4.3).

5.2.1. Rare earth elements

The analyzed serpentines display two different normalized REE patterns (Fig. 3): a flat pattern with very low HREE, and a LREE depleted pattern with mildly depleted HREE. Flat patterns are comparable to those for olivine in mantle xenoliths from British Columbia (Sun and Kerrich, 1995; Figs. 3a and 4a). The second group display REE patterns similar to those of orthopyroxene from the same xenolith suite (Figs. 3b and 4b) and those of peridotites xenoliths in Lihir (Papua New Guinea; Grégoire et al., 2001). Although the two types are quite similar in appearance, we propose that these two groups correspond to two different primary minerals: olivine for group 1 and orthopyroxene for group 2. We did not find relic clinopyroxene in our samples, which is consistent with their highly refractory composition.

5.2.2. Trace and minor elements

The contents of Ti, Y, and other elements such as Sc and Co are also different between serpentines replacing olivines and orthopyroxenes. Group 2 serpentines are enriched in Sc, Co, V, Zn, Cr, Ti, and Y compared to group 1 serpentines (Figs. 4 and 5). These elements are known to be preferentially incorporated into pyroxene. Only Ni is not consistent with this interpretation because olivine commonly contains high Ni in peridotites (≈3000 ppm; Sato, 1977; Ishimaru and Arai, 2008) and our Group 1 serpentines contain low Ni (1030 ppm in average). In contrast, group 2 serpentines contain 300 to 3000 ppm of Ni, concentrations that are typical for orthopyroxenes (Wang et al., 2008). Incorporation of Ni into Fe-oxide during the alteration of olivine would explain the relatively low Ni content of serpentines formed after olivine and varying Ni contents in Fe-oxides. Consistently high concentrations of Ni in the bulk rock samples suggest that Ni is locally mobile.

Our results suggest that, at the mineral scale, most lithophile trace elements such as REE are not (or barely) remobilized during the serpentinization process, and trace elements can be used to characterize the primary phases of serpentines. We note however that some trace elements (e.g. Ni) can be redistributed locally between secondary phases (e.g., serpentines and iron oxides).

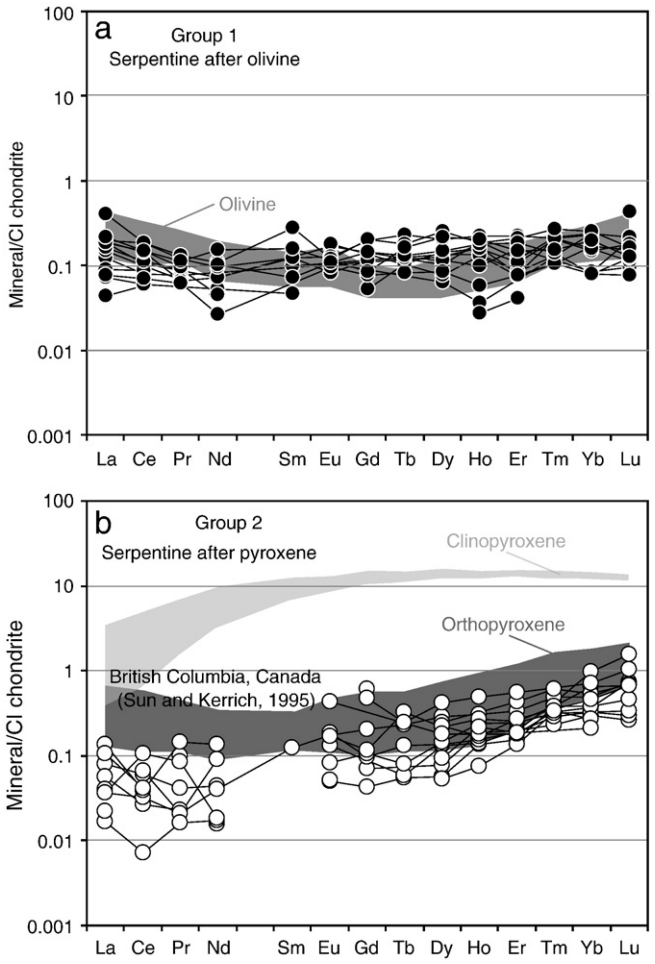

Fig. 3. a.) Chondrite normalized REE patterns for serpentine minerals after olivine (black circle — group 1) in Zildat serpentinites (CH 98A and CH 98B) analyzed by LA-HR-ICP-MS. Dark grey field are for olivine separates of ultramafic nodules from Cenozoic vents of southeastern British Columbia, Canada (Sun and Kerrich, 1995). b.) Chondrite normalized REE diagrams for serpentine minerals after pyroxene (white circle — group 2) in Zildat serpentinites (CH 98B and CH 146). Dark grey (orthopyroxene) and light grey (clinopyroxene) fields are from Sun and Kerrich (1995). Chondrite normalizing values for both diagrams were taken from McDonough and Sun (1995).

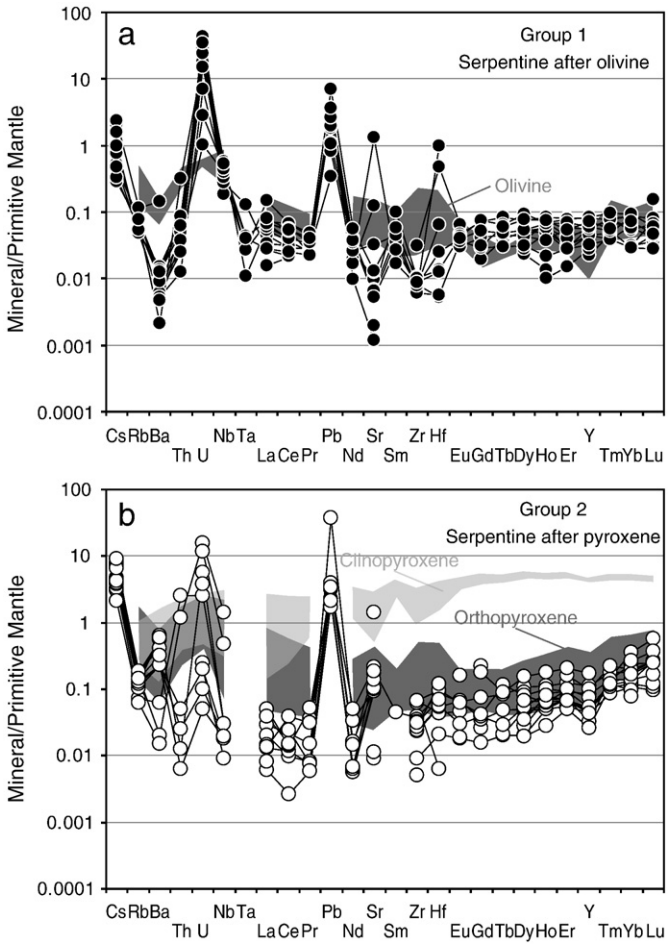

Fig. 4. Primitive mantle normalized spidergrams for a.) serpentine minerals after olivine (black circle — group 1) and b.) pyroxene (white circle — group 2) in Zildat serpentinites analyzed by LA-HR-ICP-MS. Both spidergrams are dominated by U and Pb positive anomaly. Normalizing values were taken from McDonough and Sun (1995).

5.3. Sites of highly incompatible and fluid-mobile elements in subduction-related serpentinites

Although serpentinites are recognized as the reservoir of FME (Hattori and Guillot, 2003, 2007; Tenthorey and Hermann, 2004; Savov et al., 2005b; Li and Lee, 2006), the hosting phases have not been clearly identified. Magnetite is common in serpentinites and Fe-oxide is known to adsorb cations (Takahashi et al., 2004). Hattori et al. (2005) demonstrated that, despite the presence of micrometric (<2 μm) grains of arsenide and Ni-sulfide with high As (up to 0.25 wt.%, heazlewoodite), their contribution to the whole rock budget is too small to explain high concentrations of As in serpentinites.

Despite the large size of the laser beam, some large iron oxide grains were analyzed in this study (Table 4). In agreement with previous observations by Hattori et al. (2005), their REE and FME contents are too low for them to be considered as their host and to explain the whole rock compositions. In situ data acquired on chlorite from subducted serpentinites (Cuba and Dominican Republic; Deschamps et al., 2008) do not show particular enrichment in FME.

5.3.1. Arsenic and antimony

Chalcophile elements, such as As and Sb, are moderately to highly enriched in serpentinites from supra-subduction zones (Hattori and Guillot, 2003, 2007; Savov et al., 2005a, 2007; De Hoog et al., 2008). However, compared to serpentinized peridotites from the Mariana forearc (average As = 0.355 ppm for ODP Site 780 and 0.73 ppm for ODP Site 779; Savov et al., 2005a) and from the Slovenska Bistrica ultramafic complex (average As = 3.43 ppm; De Hoog et al., 2008), serpentinites from Tso Morari contain much higher concentrations of As (average $As_{whole\ rock}$ = 51 ppm and $As_{mineral}$ = 22 ppm). Similar degrees of enrichment are observed for Sb (average $Sb_{mineral}$ = 6 ppm) in serpentine in our samples compared to the bulk rock values published by Savov et al. (2005a) (average Sb = 0.019 ppm for Site 780 and 0.0359 ppm for Site 779) and by De Hoog et al. (2008) (average Sb = 0.0958). Hattori et al. (2005) and Hattori and Guillot (2007) attributed the high As and Sb concentrations of the Tso Morari serpentinites to the composition of the subducted materials consisting in As–Sb rich marginal sediments and As–Sb depleted oceanic lithosphere. Another contributing factor is the different mineralogy of the protoliths. Serpentine that replaced olivine (group 1) show high concentrations of As (average 34 ppm) and Sb (average 11 ppm) compared to serpentine that replaced orthopyroxene (group 2; 9.3 ppm As and 0.62 ppm Sb; Fig. 6). Samples that contain high concentrations of As and Sb may have contained high abundance of olivine.

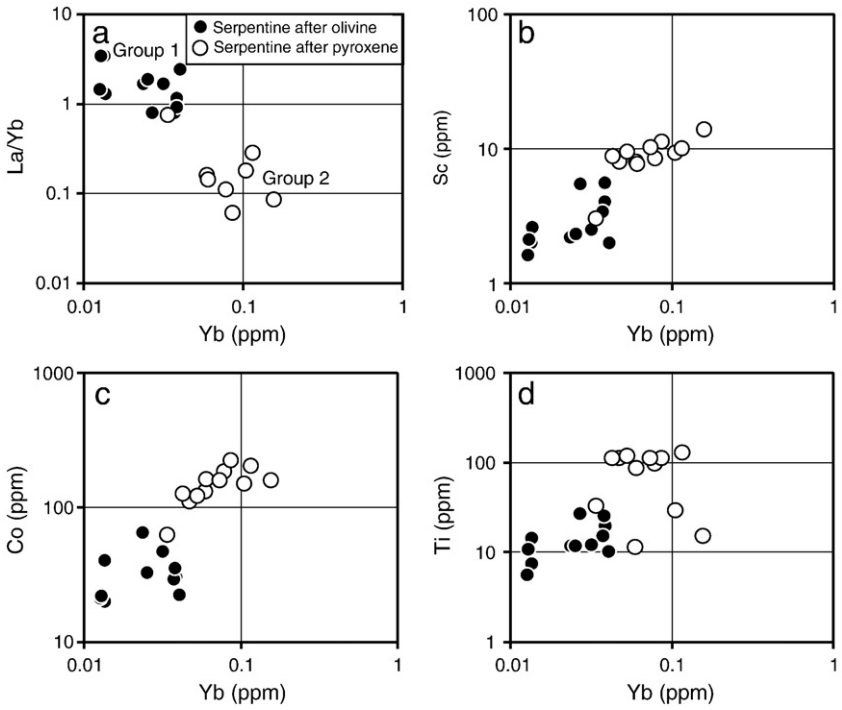

Fig. 5. Plots of La/Yb ratios and various immobile trace elements (Sc, Co, and Ti) against Yb for serpentine minerals. Distinction of primary minerals —olivine (group 1) or pyroxene (group 2) — before serpentinization events is possible with such discriminating compatible elements and HREE. All concentrations are in ppm. Symbols used are shown in insert.

5.3.2. Light elements: lithium and boron

Light elements are important tracers to evaluate element recycling in subduction zones. High concentrations of Li commonly occur in serpentinized peridotites (Parkinson and Pearce, 1998; Decitre et al., 2002; Benton et al., 2004; Savov et al., 2005a,b; Agranier et al., 2007; Savov et al., 2007; De Hoog et al., 2008) and are consistent with the elevated Li content in seawater (Li and Lee, 2006). Lithium is preferentially enriched in group 2 serpentine, i.e. serpentinized orthopyroxene (2.8–17.9 ppm), whereas Li concentrations in group 1 serpentine are low (0.29 ppm on average). The concentrations of Li in serpentinized orthopyroxenes are similar to those reported for serpentinites from other supra-subduction zone settings (3.9 to 6.3 ppm from the ODP Leg 125, Savov et al., 2005a,b; 1.44 to 29 ppm from Pohorje Mts., De Hoog et al., 2008), but higher than those observed in ophiolitic

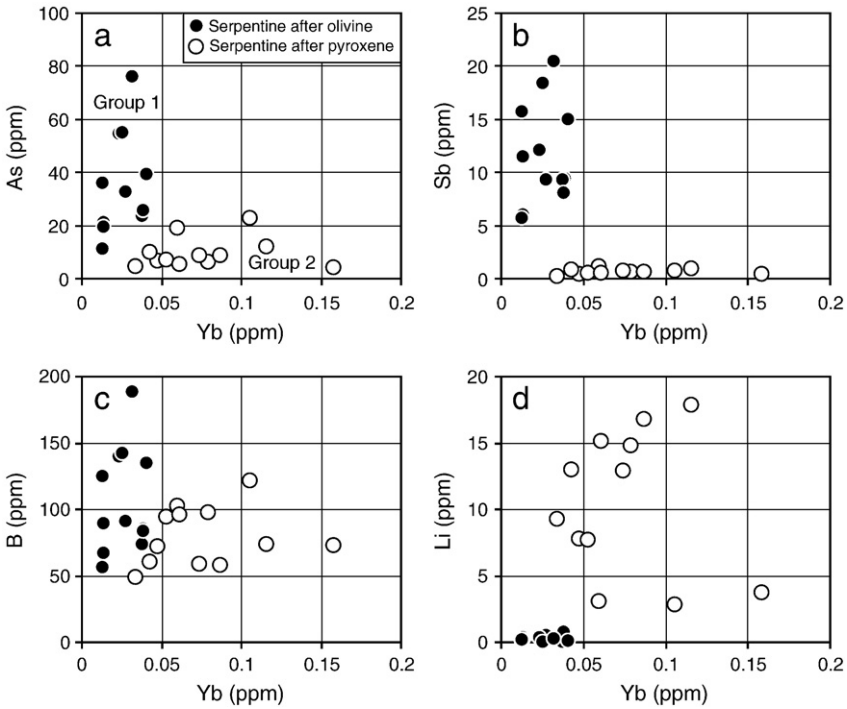

Fig. 6. Plots of FME (As, Sb, B and Li) against Yb for serpentine minerals. Yb (HREE) is used to discriminate the primary minerals. Note that serpentine minerals after olivine (group 1) display higher contents in As and Sb, whereas serpentine minerals after pyroxene (group 2) are enriched in Li. Boron concentrations are nearly identical between serpentinized olivine and pyroxene (see text). All concentrations are in ppm. Symbols used are shown in insert.

serpentinites (0.08 to 3.09 ppm, Feather River Ophiolite, Agranier et al., 2007). Recently, Vils et al. (2008) showed that Li contents of serpentine replacing olivine and orthopyroxene are comparable to those of the depleted mantle (0.7 ppm on average; Salters and Stracke, 2004). On the other hand, high concentrations of Li (10.3 ppm on average) in serpentine replacing orthopyroxene require substantial uptake of Li from fluids during the serpentinization.

The high concentrations of B (91 ppm for average of 26 samples) in whole rock of Tso Morari serpentinites are similar to those of forearc serpentinites reported from other locations (Thompson and Melson, 1970; Bonatti et al., 1984; Benton et al., 2001; Savov et al., 2005a,b, 2007; Wei et al., 2005). Compared to the concentrations of olivine and orthopyroxene (up to 0.5 ppm) reported by Vils et al. (2008), serpentines from both groups display high B concentrations probably due to interactions with fluids. In contrast to Li, B concentrations are similar in serpentinized olivine (54.1–188.2 ppm) and orthopyroxene (49–121 ppm), although the latter are slightly low (Fig. 6c).

The average B contents in the Tso Morari serpentines (91 ppm; $n=26$) are close to the values published for oceanic serpentinites (up to 139 ppm, Vils et al., 2008). The data confirm the observation of Bonatti et al. (1984) that large quantities of B (around 100 ppm) are incorporated in low-pressure serpentine polymorph. In contrast with Li, boron concentrations are independent of the primary mineralogy.

5.3.3. Uranium, thorium, and lead systematics

Primitive mantle normalized spidergrams for both groups of serpentine are characterized by positive U and Pb anomalies (Fig. 4) with no significant enrichment in Th. This is consistent with the soluble nature of U in fluids (Bailey and Ragnarsdottir, 1994). The average element abundances in serpentine are normalized to the abundances of whole rock in Fig. 7 which indicates a significant deficit in U and Pb but also in Ca and Sr. These discrepancies, especially Ca and Sr, can be explained by the occurrence of carbonate to the whole rock budget (Table 1). Carbonates are known to host U (0.142–0.655 ppm, Olivier and Boyet, 2006; 2–4 ppm; Shen and Dunbar, 1995) and Pb (0.139–3.05 ppm, Olivier and Boyet, 2006;≈9 ppm; Turekian and Wedepohl, 1961), but these concentrations are close to or higher than the values measured on serpentine minerals during this study (on average U = 0.27 and Pb = 0.6 ppm).

5.3.4. High field strength elements (Nb, Ta, Zr, and Hf)

We observed a strong fractionation of Nb (0.18 to 0.38 ppm) and Ta (0.0004 to 0.0048 ppm) showing Nb/Ta ratios ranging from 30 to 1000 in both in situ LA-HR-ICP-MS and whole rock analyses. Sample CH 146 has a Nb/Ta ratio similar to values of abyssal (Niu, 2004; Godard et al., 2008) and ophiolitic (Godard et al., 2000; Savov et al., 2005a,b; Li and Lee, 2006) peridotites and serpentinites whereas the two dunitic serpentinites, CH 98A and CH 98B, display high Nb/Ta (Fig. 8). Such a strong fractionation of Nb and Ta is rare in mantle rocks (except when carbonatitic metasomatism occurred) although it has been reported in a few samples from a spinel peridotite xenoliths

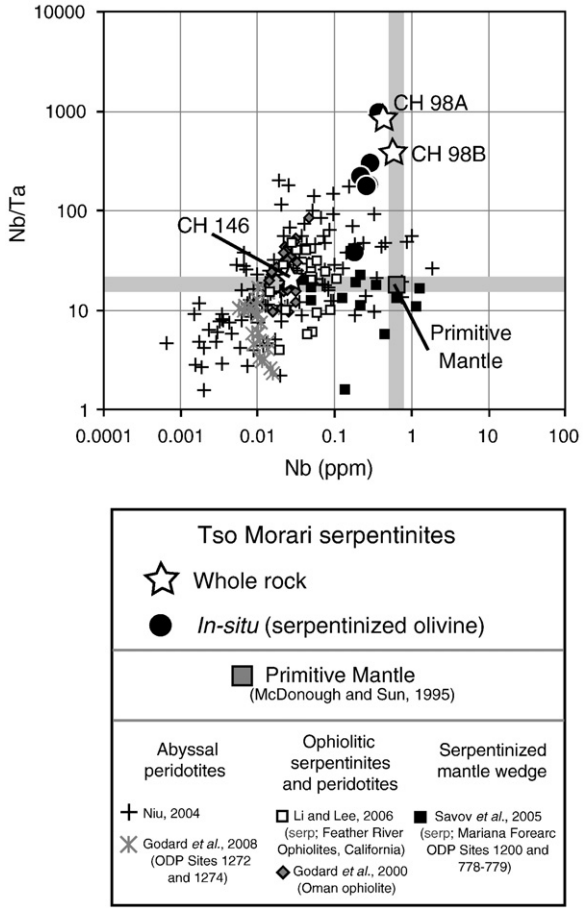

Fig. 8. Nb/Ta vs. Nb (ppm) diagram for serpentine minerals after olivine from Zildat serpentinites (black circles) and whole rock (white stars). Values for abyssal peridotites (grey diamonds; Niu, 2004), subducted and exhumed abyssal serpentinites (white squares; Li and Lee, 2006), serpentinites from Marianas hydrated mantle wedge (black squares; Savov et al., 2005a,b), and primitive mantle (grey field; McDonough and Sun, 1995) are reported for comparison. Note the strong decoupling between Nb and Ta in serpentine after olivine for samples CH 98A and CH 98B (no data available on sample CH 146 because Ta was below detection limit). See text for explanation.

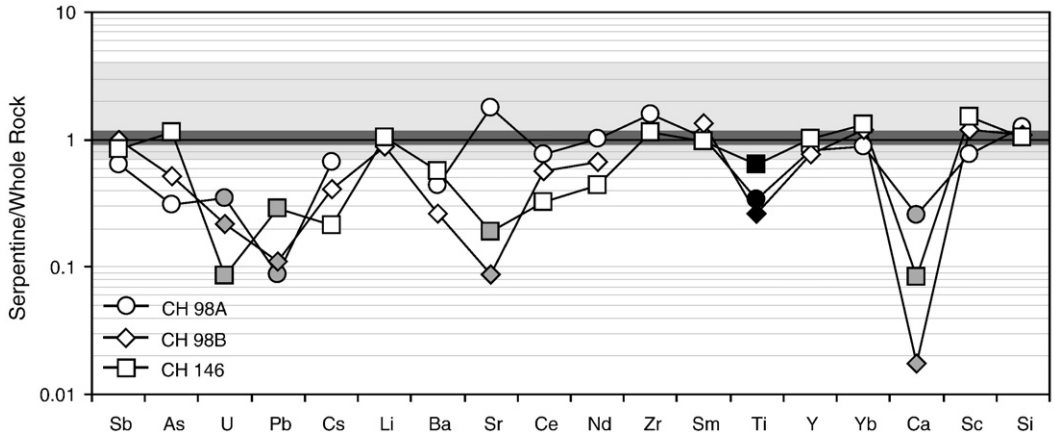

Fig. 7. Average of selected trace element abundances of serpentine minerals normalized to the trace element abundances of whole rock. Normalizing whole rock values for Si, Ca, Ti and Sb are from Hattori and Guillot (2007, pers. com.). Black points correspond to deficit elements hosted by iron oxides, whereas grey points correspond to elements probably concentrated by secondary carbonates (Ca, Sr, Pb, and U). The grey field represents a variation of ±30% relative to the whole rock.

suite from Vitim (Siberia) by Ionov et al. (2005). Samples CH 98A and 98B contain metamorphic olivine and perhaps the crystallization of clinohumite has acted as a sink for HFSE and in particular for Nb (Garrido et al., 2005). Alternatively, Nb may have been incorporated in microphases such as magnetite ferrocolumbite ($Fe^{2+}Nb_2O_6$) and pyrochlore ($(Na,Ca)_2Nb_2O_6(OH,F)$), which form in the presence of Cl− F-enriched fluids. However, the latter two are common in pegmatites and volatile-rich crustal rocks and their occurrence has not been reported in mantle rocks. Although we did not identify such phases in our samples by thin section observation, further investigations using SEM and TEM techniques are presently carried out to find HFSE-rich microphases. The remaining possibility is the incorporation of HFSE in magnetite.

5.4. Incorporation of fluid-mobile elements in the Tso Morari serpentinites: a two stage process

Two different patterns of FME distribution are observed (Fig. 9): Sb and As are preferentially incorporated in serpentine replacing olivine (10 to up to 1000 × PM), while serpentinized orthopyroxene is enriched in Pb, Cs and Li (1.5 to up to 10 × PM). B and U concentrations are relatively similar in both types of serpentines.

The different distribution of FME in serpentines can be related to (i) the composition of primary minerals or (ii) the temperatures of the serpentinization of these minerals in the mantle wedge. In our samples, the different enrichment patterns for FME are related to different primary minerals, as already demonstrated for some compatible elements and for REE. Because of the strong FME enrichments observed in both types of Tso Morari serpentines relative to ophiolitic serpentinites (Savov et al., 2005a,b; Li and Lee, 2006) and to the mantle peridotites (e.g. McDonough and Sun, 1995; Lyubetskaya and Korenaga, 2007; Salters and Stracke, 2004), we suggest that FME were added to the serpentines during the hydration, and that the variable FME enrichments are not related to primary phase compositions. As the mobility of FME and the stability of primary minerals vary with temperature, serpentinization at different temperatures affected the distribution of FME.

Observations of natural samples (Mével, 2003) and experimental works (Martin and Fyfe, 1970; Allen and Seyfried, 2003) indicate that olivine is easily destabilized at low temperatures (<300 °C; Allen and Seyfried, 2003; Hattori and Hamilton, 2008), according to the reaction (O'Hanley, 1996):

$$\text{Forsterite} + \text{Water} = \text{Brucite} + \text{Serpentine}$$

$$2Mg_2SiO_4 + 3H_2O = Mg(OH)_2 + Mg_3Si_2O_5(OH)_4$$

Therefore, assuming that the hydrated mantle wedge is pulled downward due to subduction (e.g. Furukawa, 1993), serpentinization of olivine takes place at shallow depths and it incorporates the elements released from the slab in the earliest stage of subduction (Fig. 10). High concentrations in Sb and As observed in serpentine after olivine (Fig. 9) compared to serpentinized pyroxene suggest that they are incorporated at temperatures below 300 °C (Fig. 10). This observation is consistent with the conclusions of Hattori et al. (2005), Savov et al. (2005a), and Savov et al. (2007).

Then, the increasing temperature with increasing depth results in the serpentinization of orthopyroxene. Above 400 °C, the dissolution reaction destabilized orthopyroxene (Martin and Fyfe, 1970; Oelkers and Schott, 2001; Allen and Seyfried, 2003), following the reaction:

$$\text{Enstatite} + \text{Water} = \text{Serpentine} + \text{Talc}$$

$$6MgSiO_3 + 3H_2O = Mg_3Si_2O_5(OH)_4 + Mg_3Si_4O_{10}(OH)_2$$

As the slab is hotter at deeper levels, it releases elements such as Pb, Cs, and Li, that will be incorporated preferentially into the serpentinized pyroxene (Fig. 10).

The following elements are known to be mobile in aqueous fluids for temperature ranging between room temperature and 500 °C. Arsenic and antimony are soluble in aqueous fluids at low temperature, as observed with the high concentrations of As in surface and ground waters (Rose et al., 1979; Smedley and Kinniburgh, 2002; Takahashi et al., 2004). Previous studies based on the oxidation state of As using X-ray absorption near-edge structure spectra have showed "that As^{5+} was transferred by aqueous fluids from a slab under oxidized conditions at shallow depths, <25 km (Hattori et al., 2005)". Thereby, As and Sb are released at shallow depths from the slab and then are incorporated in the serpentinite layer. Boron is known to be incorporated in peridotites

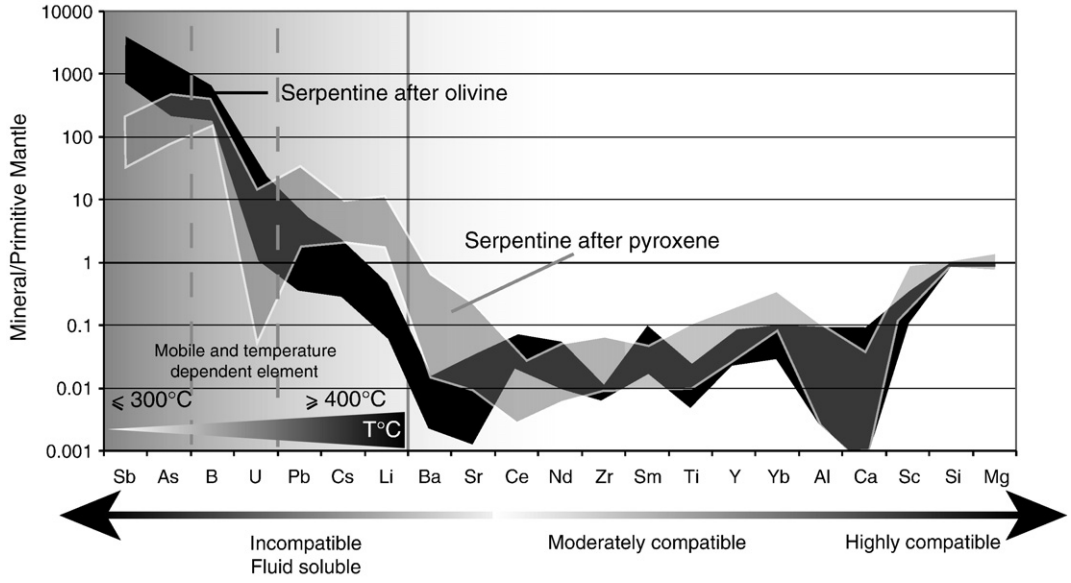

Fig. 9. Normalized concentrations (McDonough and Sun, 1995) of fluid-mobile and fluid-immobile elements in serpentine minerals deriving from primary olivine (black field) or from primary orthopyroxene (grey field) in Zildat serpentintes. Diagram modified from Hattori and Guillot (2003, 2007). Note the decoupled enrichment between serpentinized olivine (Sb, As, and U rich) and serpentinized pyroxene (Pb, Cs, Li, Ba, Sr rich). Boron shows nearly constant contents despite the nature of the primary minerals.

for temperature below 300 °C (Seyfried and Dibble, 1980) and, as a consequence, presents a behavior close to As and Sb.

We suggest that the behavior of FME in serpentinized mantle wedge is intimately coupled with the differential discharge of these same elements from the slab. Sb and As are found to be excellent tracers of the serpentinization of olivine at low temperature (<300 °C) in the Tso Morari serpentinites. We propose that the enrichment of Pb, Cs, and Li represents the second stage of serpentinization of pyroxene at higher temperature (~400 °C). Studies on high-pressure (HP) and UHP metabasaltic and metasedimentary rocks showed increasing mobility of lithophile elements (LILE, U, Th, Pb, and Li) at depth of about 90 km (Bebout, 2007), which corresponds to temperatures ≥400 °C (epidote-blueschist facies; Bebout et al., 1999) along a cold subduction geotherm (Fukao et al., 1983; Furukawa, 1993; Peacock and Wang, 1999). Li is known to be incorporated in minerals at low temperature (≤150 °C in smectites and chlorites, Decitre et al., 2002; ≤350 °C in serpentine, Seyfried et al., 1998), although it is released from basalts at temperatures (>250 °C) higher than that for the release of K, Rb, and Cs. The deeper release of Li from slab explains its late incorporation in the overlying mantle wedge.

The serpentinization of orthopyroxene starts to take place at around 300–400 °C (Fig. 9). Therefore, B and U are incorporated equally in both types of serpentine. We know of the existence of serpentinites samples where unaltered olivine coexists with serpentinized orthopyroxene (Hess Deep, Stamoudi, 2002), indicating that serpentinization took place at temperatures higher than 400 °C. It is not the case of our samples where both olivine and pyroxene were destabilized, showing two distinct geochemical signatures, and consequently corresponding to two distinct serpentinization events. This geochemical observation suggests that serpentinization accompanied by the incorporation of FME occurred during temperature increase, which is compatible with the progressive burial of serpentinite layer along the subduction plane (e.g., Bostock et al., 2002; Gorczyk et al., 2007; Fig. 10). The preservation of two different

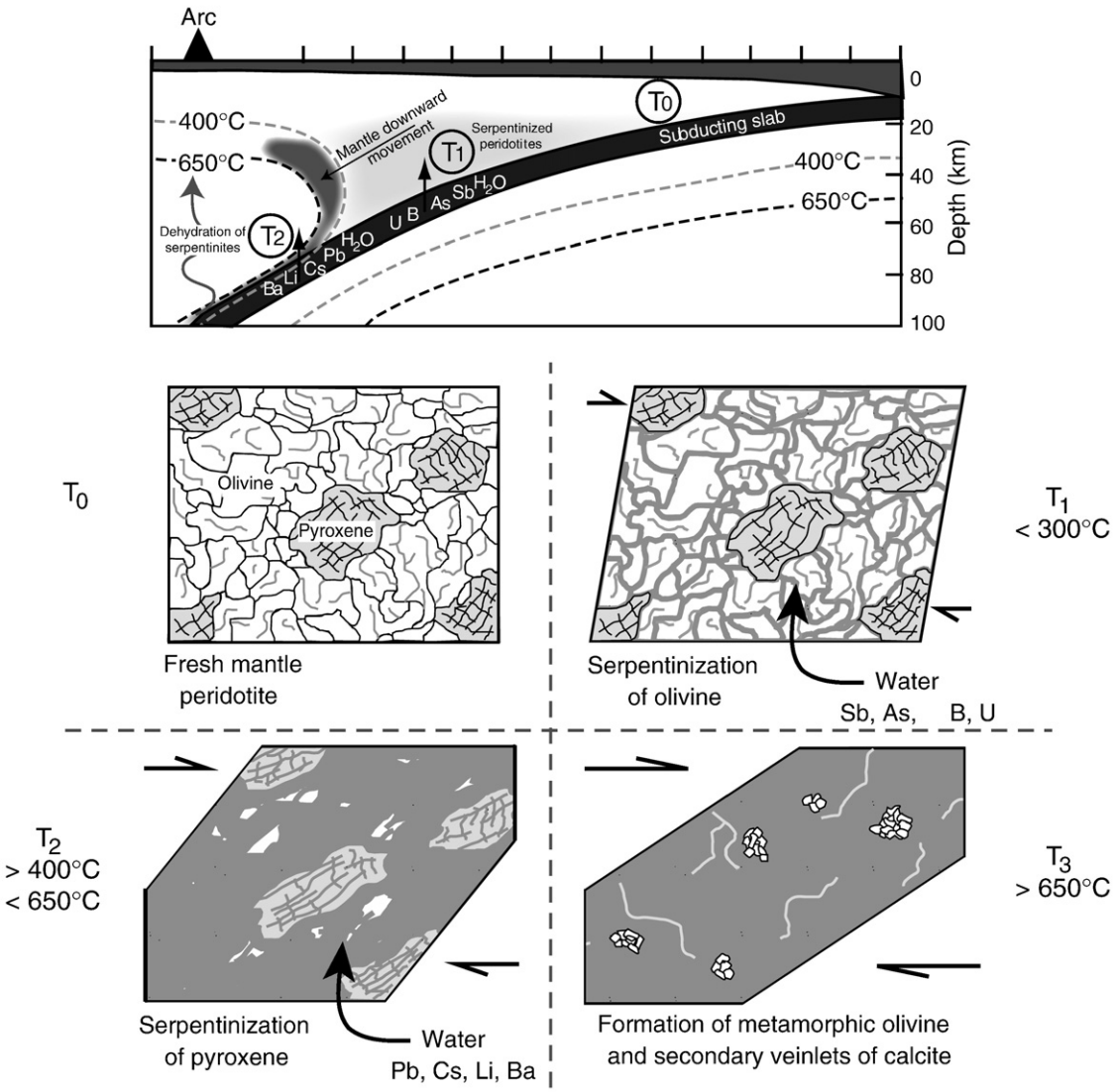

Fig. 10. Schematic sketch to illustrate the "two-times" enrichment in FME on serpentine minerals. Thermal structure for a cool continental subduction zone is from Hyndman and Peacock (2003). T_0 (time 0) illustrates the peridotite protolithe of Tso Morari serpentinites with olivine and pyroxene. (T_1) is the first step of serpentinization inside the mantle wedge with destabilization of primary olivine at temperature below 300 °C (Allen and Seyfried, 2003) and incorporation of the most FME (Sb, As, B and U). Thus, with increasing temperature at T_2, orthopyroxene is destabilized (>400 °C–<650 °C) and takes up mobile elements such as Pb, Cs, Li and Ba. The final stage (T_3) corresponds to sheared serpentinites containing metamorphic olivine (Guillot et al., 2001). This thermal destabilization of serpentine occurs at temperature higher than 650 °C (Wunder et al., 2001). Note the continuous deformation recorded by serpentinites during the downward movement and exhumation that erases the primary textures.

patterns for FME depending on the primary minerals suggests that these elements were not or little remobilized during late high temperature and/or retrograde metamorphism.

5.5. Himalayan serpentinites: particular case of metasomatised mantle wedge?

The peridotites from mantle wedges are generally highly refractory and serpentinites deriving from these rocks preserve the depleted REE signature of their protoliths. Hence, serpentinized harzburgite and dunite from Izu–Bonin–Marianna (IBM) arc system (Fig. 1) represent a strongly depleted upper mantle peridotites later metasomatized by fluids derived from the subducting Pacific Ocean plate (Parkinson and Pearce, 1998; Savov et al., 2005a,b, 2007). The enrichment is observed for FME such as B (4–60 ppm), Li (0.4–18 ppm), As (0.1–2.5 ppm), Sb (0.001–0.258 ppm), Sr (1.6–40.8 ppm), Cs (0.02–1.2 ppm), Ba (1–13 ppm), and U (up to 0.0026 ppm) (Savov et al., 2005a,b, 2007). Located in an intra-oceanic setting, the IBM forearc shows no geophysical evidence for an accretionary prism (Horine et al., 1990; Fryer, 1996; Fryer et al., 1999), and the layer of sediments entering into the subduction zones is thin (around 400 m; Chauvel et al., 2009).

The detailed tectonic and geochemical study of the Tso Morari serpentinites indicates that they derive from a refractory mantle wedge (Guillot et al., 2001; Hattori and Guillot, 2007). Yet, two main characteristics distinguish the Tso Morari serpentinites from peridotites and serpentinites considered as representative of the mantle wedge composition, such as those sampled in the IBM forearc (Parkinson and Pearce, 1998; Savov et al., 2005a). First, the Tso Morari serpentinites contain relatively high concentrations of elements that are not mobile in aqueous fluids, such as Nb or REE, compared to serpentinites from the IBM forearc (Parkinson and Pearce, 1998; Savov et al., 2005a; Fig. 1a). In situ analyses indicate that the serpentine compositions are very similar to that of fresh olivine and orthopyroxene observed in unaltered but metasomatized mantle peridotites (Sun and Kerrich, 1995). This led us to posit that these elemental enrichments did not occur during serpentinization but characterized the unaltered protolith of the Tso Morari serpentinites. This assumption is consistent with the results of our Pb isotope compositions that indicate that this protolith derive from a mantle having a composition different from that of a pristine depleted mantle (Fig. 2). Previous structural and geochemical studies carried out in the Ladakh area have shown that this region record a series of intra-oceanic subductions, which are accompanied by extensive metasomatism of the underlying mantle. Mahéo et al. (2004) show that the peridotites from Spontang and Nidar ophiolites (located nearby the Tso Morari region in the Ladakh area) derive from a depleted N-MORB mantle later metasomatised and selectively enriched in trace elements by the injection of tholeiitic magmas in the intra-oceanic arc setting. A similar metasomatic process likely affected the protolith of the Tso Morari serpentinites. Our geochemical data support their scenario, in which the mantle wedge above the Indian slab sampled a refractory yet metasomatized oceanic mantle, in contrast to that sampled today in intra-oceanic subduction settings (e.g. the IBM forearc).

Second, the Tso Morari serpentinites are selectively enriched in some FME (Sb, As and to a lesser extent B) compared to the IBM serpentinites, although Li, Cs, Sr, Rb, Ba, and U show similar degrees of enrichment. We propose that the latter elements derive mainly from fluids released from Tethyan oceanic rocks that are enriched in these elements during seawater interaction at the sea floor. This interpretation is in agreement with the high contents of these elements in seawater (Li and Lee, 2006). In contrast Sb and As (and probably B) would come from a sedimentary source. An accretionary wedge is lacking in IBM whereas an accretionary wedge was developed in the Tso Morari area (Guillot et al., 2008). As suggested by Hattori and Guillot (2007) and our new Pb isotopes, the observed enrichments can be attributed to the presence of large quantities of sediments, clasts of which were originated from Archean lithologies (Fig. 2). These sediments are enriched in chalchophile elements (Mohan et al., 2008).

Thus, Tso Morari serpentinites present hydrated mantle peridotites that were metasomatized and later serpentinized by FME-rich fluids deriving from both oceanic lithosphere and continental lithologies.

6. Conclusion

Serpentinites deriving from the hydration of mantle wedge display strong enrichments in fluid-mobile elements. In the case of the Tso Morari serpentinites, these elements are transferred to the mantle wedge by aqueous fluids deriving from oceanic lithosphere, oceanic sediments, and sediments deposited on the margin of the Indian continent. Lead isotopic signatures are similar to those of arc volcanics in the area and attributed to the mantle wedge contaminated by the subducted materials (subducted sediments and Archean lithologies of the Indian margin). The serpentinites act as a "sponge", transferring isotopic characteristics from shallower to deeper and hotter levels in the mantle, down to the isotherm 600–650 °C where dehydration occurs.

Based on the chemical composition of serpentine determined by in situ analysis technique, we propose the following salient results:

(1) Compatible and rare earth elements may characterize the primary minerals (olivine or orthopyroxene) after which serpentines were formed.
(2) Serpentine displays large enrichments in FME (Sb, As, B, U, Pb, Cs, and Li), confirming the observations made previously on the whole rocks. These elements are concentrated in serpentine minerals; no enrichment is observed in the associated Fe-oxides. However, the distribution of FME depends on the primary minerals. Sb and As are mainly concentrated in serpentine replacing olivine, whereas serpentine deriving from orthopyroxene concentrates preferentially Pb, Cs, and Li. B and U are identically incorporated in both kinds of serpentine.
(3) The disparity in the distribution of FME in serpentine results both from differential release of FME from the slab and a temperature change during serpentinization event in the descending mantle wedge coupled to the slab. Thus, the elements released early from the slab (Sb and As) are incorporated in serpentine after olivine at temperature below 300 °C. Later, Pb, Cs, and Li are released from the downward slab as it reaches a temperature above 400 °C and they are incorporated into serpentine replacing orthopyroxene.

Acknowledgments

We thank Nicolas Geoffroy (LGIT Grenoble) for the interpretation of X-ray diffraction patterns, Jean-Luc Devidal (Magmas et Volcans Clermont-Ferrand) for microprobe analyses, Simone Pourtales and Olivier Bruguier (Géosciences Montpellier) for their help during (LA-) HR-ICP-MS analyses, and Adeline Besnault (LGCA Grenoble) for Pb isotope dilution and analyses. We are grateful to Michel Grégoire, Bruno Dhuime, and Bernd Wunder for their constructive scientific discussions. This paper has been improved by G.E. Bebout, B. Bourdon and an anonymous reviewer. The research project was supported by PROCOPE grant and CNRS INSU programs.

Appendix A. Supplementary data

Supplementary data associated with this article can be found, in the online version, at doi:10.1016/j.chemgeo.2009.10.002.

References

Agranier, A., Lee, C.-T.A., Li, Z.-X.A., Leeman, W.P., 2007. Fluid mobile element budgets in serpentinized oceanic lithospheric mantle: insights from B, As, Li, Pb, PGEs and Os isotopes in the Feather River Ophiolite, California. Chemical Geology 245, 230–241.

Allen, D.E., Seyfried Jr., E., 2003. Compositional controls on vent fluids from ultramafic-hosted hydrothermal systems at mid-ocean ridges: an experimental study at 400 °C, 500 bars. Geochimica et Cosmochimica Acta 67 (8), 1531–1542.
Bailey, E.H., Ragnarsdottir, K.V., 1994. Uranium and thorium solubilities in subduction zone fluids. Earth and Planetary Science Letters 124, 119–129.
Bebout, G.E., 2007. Metamorphic chemical geodynamics of subduction zones. Earth and Planetary Science Letters 260, 373–393.
Bebout, G.E., Ryan, J.G., Leeman, W.P., Bebout, A.E., 1999. Fractionation of trace elements by subduction-zone metamorphism — effect of convergent-margin thermal evolution. Earth and Planetary Science Letters 171, 63–81.
Ben Othman, D., White, W.M., Patchett, J., 1989. The geochemistry of marine sediments, island arc magma genesis, and crust-mantle recycling. Earth and Planetary Science Letters 94, 1–21.
Benton, L.D., Ryan, J.G., Savov, I.P., 2004. Lithium abundance and isotope systematics of forearc serpentinites, Conical Seamount, Mariana forearc: insights into the mechanics of slab-mantle exchange during subduction. Geochemistry Geophysics Geosystems 5 (8). doi:10.1029/2004GC000708.
Benton, L.D., Ryan, J.G., Tera, F., 2001. Boron isotopes systematics of slab fluids as inferred from a serpentine seamount, Mariana forearc. Earth and Planetary Science Letters 187, 273–282.
Blakely, R.J., Brocher, T.M., Wells, R.E., 2005. Subduction zone magnetic anomalies and implications for hydrated forearc mantle. Geology 3, 445–448.
Blichert-Toft, J., Weis, D., Maerschalk, C., Agranier, A., Albarède, F., 2003. Hawaïan hotspot dynamics as inferred from the Hf and Pb isotope evolution of Mauna Kea volcano. Geochemistry Geophysics Geosystems 4 (2). doi:10.1029/2002GC000340.
Bonatti, E., Lawrence, J.R., Morandi, N., 1984. Serpentinization of oceanic peridotites: temperature dependence of mineralogy and boron content. Earth and Planetary Science Letters 70, 88–94.
Bostock, M.G., Hyndman, R.D., Rondenay, S., Peacock, S.M., 2002. An inverted continental Moho and serpentinization of the forearc mantle. Nature 417, 536–538.
Brocher, T.M., Parsons, T., Trehu, A.M., Snelson, C.M., Fisher, M.A., 2003. Seismic evidence for widespread serpentinized forearc upper mantle along the Cascadia margin. Geology 31, 267–270.
Chakrabarti, R., Basu, A.R., 2006. Trace element and isotopic evidence for Archean basement in the Lonar crater impact breccia, Deccan Volcanic Province. Earth and Planetary Science Letters 247, 197–211.
Chalot-Prat, F., Ganne, J., Lombard, A., 2003. No significant element transfer from the oceanic plate to the mantle wedge during subduction and exhumation of the Tethys lithosphere (Western Alps). Lithos 69, 69–103.
Chauvel, C., Marini, J.-C., Plank, T., Ludden, J.N., 2009. Hf–Nd input flux in the Izu–Mariana subduction zone and recycling of subducted material in the mantle. Geochemistry Geophysics Geosystems 10 (1). doi:10.1029/2008GC002101.
Coleman, R.G., Keith, T.E., 1971. A chemical study of serpentinization — Burro Mountain, California. Journal of Petrology 12 (2), 311–328.
Decitre, S., Deloule, E., Reisberg, L., James, R., Agrinier, P., Mével, C., 2002. Behaviour of Li and its isotopes during serpentinization of oceanic peridotites. Geochemistry Geophysics Geosystems 3 (1). doi:10.1029/2001GC000178.
De Hoog, J.C.M., Janàk, M., Vrabec, M., Froitzheim, N., 2008. Serpentinised peridotites from an ultrahigh-pressure terrane in the Pohorje Mts. (Eastern Alps, Slovenia): geochemical constraints on petrogenesis and tectonic setting. Lithos 109, 209–222.
Deschamps, F., Guillot, S., Godard, M., Andreani, M., 2008. In situ characterization of subduction-related serpentinites: a new vision on behaviour of fluid mobile elements during the subduction factory. Geophysical Research abstracts EGU 2008 10, EGU2008-A-08786.
De Sigoyer, J., Guillot, S., Dick, P., 2004. Exhumation of the ultra-high pressure Tso Morari unit in eastern Ladakh (NW Himalaya): a case study. Tectonics 23, TC3003. doi:10.1029/2002TC00001492.
Dhuime, B., Bosch, D., Bodinier, J.-L., Garrido, C.J., Bruguier, O., Hussain, S.S., Dawood, H., 2007. Multistage evolution of the Jijal ultramafic–mafic complex (Kohistan, N Pakistan): implications for building the roots of island arcs. Earth and Planetary Science Letters 261, 179–200.
Dungan, M., 1979. Bastite pseudomorphs after orthopyroxene, clinopyroxene and tremolite. Canadian Mineralogist 17, 729–740.
Evans, B.W., 1977. Metamorphism of alpine peridotite and serpentinite. Annual Reviews of Earth and Planetary Sciences 5, 397–447.
Fryer, P., 1996. Evolution of the Mariana convergent plate margin system. Reviews of Geophysics 34 (1), 89–125.
Fryer, P., Wheat, C.G., Mottl, M.J., 1999. Mariana blueschist mud volcanism: implications for conditions within the subduction zone. Geology 27, 103–106.
Fukao, Y., Hori, S., Ukawa, M., 1983. A seismological constraint on the depth of basalt–eclogite transition in a subducting ocenic crust. Nature 303, 413–415.
Furukawa, Y., 1993. Depth of the decoupling plate interface and thermal structure under arcs. Journal of Geophysical Research 98, 20,005–20,013.
Galer, S.J.G., Abouchami, W., 1998. Practical application of lead triple spiking for correction of instrumental mass discrimination. Mineralogical Magazine 62A, 491–492.
Garrido, C.J., López Sánchez-Vizcaíno, V., Gómez-Pugnaire, M.T., Trommsdorff, V., Alard, O., Bodinier, J.-L., Godard, M., 2005. Enrichment of HFSE in chlorite–harzburgite produced by high-pressure dehydration of antigorite–serpentinite: implications for subduction magmatism. Geochemistry Geophysics Geosystems 6 (1). doi:10.1029/2004GC000791.
Godard, M., Lagabrielle, Y., Alard, O., Harvey, J., 2008. Geochemistry of the highly depleted peridotites drilled at ODP Sites 1272 and 1274 (Fifteen-Twenty Fracture Zone, Mid-Atlantic Ridge): implications for mantle dynamics beneath a slow spreading ridge. Earth and Planetary Science Letters 267, 410–425.
Godard, M., Jousselin, D., Bodinier, J.-L., 2000. Relationships between geochemistry and structure beneath a palaeo-spreading centre: a study of the mantle section in the Oman Ophiolite. Earth and Planetary Science Letters 180, 133–148.
Gorczyk, W., Guillot, S., Gerya, T.V., Hattori, K., 2007. Asthenospheric upwelling, oceanic slab retreat, and exhumation of UHP mantle rocks: insights from Greater Antilles. Geophysical Research Letters 34. doi:10.1029/2007GL031059.
Govindaraju, K., 1994. 1994 compilation of working values and sample description for 383 geostandards. Geostandards Newsletters 18, 1–158 Sp. Issue.
Grégoire, M., McInnes, B.I.A., O'Reilly, S.Y., 2001. Hydrous metasomatism of oceanic sub-arc mantle, Lihir, Papua New Guinea. Part 2. Trace element characteristics of slab-derived fluids. Lithos 59, 91–108.
Guillot, S., Mahéo, G., De Sigoyer, J., Hattori, K.H., Pêcher, A., 2008. Tethyan and Indian subduction viewed from the Himalayan high- to ultrahigh-pressure metamorphic rocks. Tectonophysics 451, 225–241.
Guillot, S., Garzanti, E., Baratoux, D., Marquer, D., Mahéo, G., De Sigoyer, J., 2003. Reconstructing the total shortening history of the NW Himalaya. Geochemistry Geophysics Geosystems. doi:10.1029/2002GC000484.
Guillot, S., Hattori, K.H., De Sigoyer, J., Nägler, T., Auzende, A.-L., 2001. Evidence of hydration of the mantle wedge and its role in the exhumation of eclogites. Earth and Planetary Science Letters 193, 115–127.
Guillot, S., Hattori, K., De Sigoyer, J., 2000. Mantle wedge serpentinization and exhumation of eclogites: insights from eastern Ladakh, northwest Himalaya. Geology 28, 199–202.
Gunther, D., Heinrich, C.A., 1999. Enhanced sensitivity in laser ablation-ICP mass spectrometry using helium–argon mixtures as aerosol carrier — plenary lecture. Journal of Analytical Atomic Spectrometry 14 (9), 1363–1368.
Hart, S.R., 1984. A large-scale isotopic anomaly in the Southern Hemisphere mantle. Nature 309, 753–757.
Hattori, K.H., Hamilton, S., 2008. Geochemistry of peat over kimberlites in the Attawapiskat area, James Bay Lowlands, northern Canada. Applied Geochemistry 23, 3767–3782.
Hattori, K.H., Guillot, S., 2007. Geochemical character of serpentinites associated with high- to ultrahigh-pressure metamorphic rocks in the Alps, Cuba, and the Himalayas: recycling of elements in subduction zones. Geochemistry Geophysics Geosystems 8 (9). doi:10.1029/2007GC001594.
Hattori, K., Takahashi, Y., Guillot, S., Johanson, B., 2005. Occurrence of arsenic (V) in forearc mantle serpentinites based on X-ray absorption spectroscopy study. Geochimica et Cosmochimica Acta 69 (23), 5585–5596.
Hattori, K.H., Guillot, S., 2003. Volcanic fronts form as a consequence of serpentinite dehydration in the forearc mantle wedge. Geology 31 (6), 525–528.
Horine, R.L., Moore, G.F., Taylor, B., 1990. Structure of the outer Izu–Bonin forearc from seismic-reflection profiling and gravity modelling. Proceeding of Ocean Drilling Program Initial Report 125, 81–94.
Hyndman, R.D., Peacock, S.M., 2003. Serpentinization of the forearc mantle. Earth and Planetary Science Letters 212, 417–432.
Ionov, D.A., Ashchepkov, I., Jagoutz, E., 2005. The provenance of fertile off-craton lithospheric mantle: Sr–Nd isotope and chemical composition of garnet and spinel peridotite xenoliths from Vitim, Siberia. Chemical Geology 217, 41–75.
Ionov, D.A., Savoyant, L., Dupuy, C., 1992. Application of the ICP-MS technique to trace element analysis of peridotites and their minerals. Geostandard Newsletters 16, 311–315.
Ishimaru, S., Arai, S., 2008. Nickel enrichment in mantle olivine beneath a volcanic front. Contributions to Mineralogy and Petrology 156, 119–131.
Jochum, K.P., Seufert, H.M., Thirwall, M.F., 1990. High-sensitivity Nb analysis by spark-source mass spectrometry (SSMS) and calibration of XRF Nb and Zr. Chemical Geology 81, 1–16.
Jochum, K.P., Willbold, M., Raczek, I., Stoll, B., Herwig, K., 2005. Chemical characterisation of the USGS reference glasses GSA-1G, GSC-1G, GSD-1G, GSE-1G, BCR-2G, BHVO-2G and BIR-1G using EPMA, ID-TIMS, ID-ICPMS and LA-ICPMS. Geostandards and Geoanalytical Research 29 (3), 285–302.
Jochum, K.P., Stoll, B., 2008. Reference materials for elemental and isotopic analyses by LA-(MC)-ICP-MS: successes and outstanding needs. In: Sylvester, P. (Ed.), Laser ablation ICP-MS in the Earth Sciences: current practices and outstanding issues: Mineralogical Association Canada, pp. 147–168.
Kamiya, S., Kobayashi, Y., 2000. Seismological evidence for the existence of serpentinized wedge mantle. Geophysical Research Letters 27 (6), 819–822.
Komor, S.C., Elthon, D., Casey, J.F., 1985. Serpentinization of cumulate ultramafic rocks from the North Arm Mountain massif of the Bay of Islands ophiolite. Geochimica et Cosmochimica Acta 49, 2331–2338.
Leeman, W.P., 1996. Boron and other fluid-mobile elements in volcanic arc lavas: implications for subduction processes. Subduction top to bottom: In: Bebout, G. E., et al. (Ed.), American Geophysical Union Geophysical Monograph, vol. 96, pp. 269–276.
Li, Z.-X.A., Lee, C.-T.A., 2006. Geochemical investigation of serpentinized oceanic lithospheric mantle in the Feather River Ophiolite, California: implications for the recycling rate of water by subduction. Chemical Geology 235, 161–185.
Lyubetskaya, T., Korenaga, J., 2007. Chemical composition of Earth's primitive mantle and its variance: 1. Method and results. Journal of Geophysical Research 112 (B03211). doi:10.1029/2005JB004223.
Mahéo, G., Bertrand, H., Guillot, S., Villa, I.M., Keller, F., Capiez, P., 2004. The South Ladakh ophiolites (NW Himalaya, India): an intra-oceanic tholeiitic arc origin with implications for the closure of the Neo-Tethys. Chemical Geology 203, 273–303.
Mahoney, J.J., Graham, D.W., Christie, D.M., Johnson, K.T.M., Hall, L.S., Vonderhaar, D.L., 2002. Between a hotspot and a cold spot: isotopic variation in the Southeast Indian Ridge asthenosphere, 86 E–118 E. Journal of Petrology 43 (7), 1155–1176.

Mahoney, J.J., Frei, R., Tejada, M.L.G., Mo, X.X., Leat, P.T., Nägler, T.F., 1998. Tracing the Indian Ocean mantle domain through time: isotopic results from old west Indian, east tethyan, and south pacific seafloor. Journal of Petrology 39 (7), 1285–1306.
Manhès, G., Allègre, C.J., Provost, A., 1984. U–Th–Pb systematics of the eucrite "Juvinas": precise age determination and evidence for exotic lead. Geochimica et Cosmochimica Acta 48, 2247–2264.
Martin, B., Fyfe, W.S., 1970. Some experimental and theoretical observations on the kinetics of hydration reactions with particular reference to serpentinization. Chemical Geology 6, 185–202.
McDonough, W.F., Sun, S.-S., 1995. The composition of the Earth. Chemical Geology 120, 223–253.
Menzies, M.A., Long, A., Ingram, G., Tatnell, M., Janecky, D., 1993. MORB peridotite–seawater interaction: experimental constraints on the behaviour of trace elements, $^{87}Sr/^{86}Sr$ and $^{143}Nd/^{144}Nd$ ratios. In: Prichard, H.M., Alabaster, T., Harris, N.B.W., Neary, C.R. (Eds.), Magmatic Processes and Plate Tectonics: Geological Society Special Publication, vol. 76, pp. 309–322.
Mével, C., 2003. Serpentinization of abyssal peridotites at mid-ocean ridges. Comptes Rendus Géoscience 335, 825–852.
Miller, C., Schuster, R., Klötzli, U., Frank, W., Purtscheller, F., 1999. Post-collisional potassic and ultrapotassic magmatism in SW Tibet: geochemical and Sr–Nd–Pb–O isotopic constraints for mantle source characteristics and petrogenesis. Journal of Petrology 40 (9), 1399–1424.
Miyashiro, A., Shido, F., Ewing, M., 1969. Composition and origin of serpentinites from the Mid-Atlantic Ridge near 24 and 30 N. Contributions to Mineralogy and Petrology 23, 117–127.
Mohan, R.M., Kamber, B.S., Piercey, S.J., 2008. Boron and arsenic in highly evolved Archean felsic rocks: implications for Archean subduction processes. Earth and Planetary Science Letters 274, 479–488.
Moll, M., Paulick, H., Suhr, G., Bach, W., 2007. Data report: microprobe analyses of primary phases (olivine, pyroxene, and spinel) and alteration products (serpentine, iowaite, talc, magnetite, and sulfides) in Holes 1268A, 1272A, and 1274A. In: Kelemen, J., Kikawa, E., Miller, D.J. (Eds.), Scientific Results of Ocean Drilling Program Leg 209. TAMU, College Station TX, USA, p. 209.
Niu, Y., 2004. Bulk-rock major and trace element compositions of abyssal peridotites: implications for mantle melting, melt extraction and post-melting processes beneath Mid-Ocean Ridges. Journal of Petrology 45 (12), 2423–2458.
Noll Jr., P.D., Newsom, H.E., Leeman, W.P., Ryan, J.G., 1996. The role of hydrothermal fluids in the production of subduction zone magmas: evidence from siderophile and chalcophile trace elements and boron. Geochimica et Cosmochimica Acta 60, 587–611.
O'Brien, P., Zotoy, N., Law, R., Kahn, A.M., Jan, M.Q., 2001. Coesite in Himalayan eclogite and implication for models of India-Asia collision. Geology 29, 435–438.
O'Hanley, D.S., 1996. Serpentinites, records of tectonic and petrological history. Oxford Monographs on Geology and Geophysics (34).
Oelkers, H., Schott, J., 2001. An experimental study of enstatite dissolution rates as a function of pH, temperature, and aqueous Mg and Si concentration, and the mechanism of pyroxene/pyroxenoid dissolution. Geochimica et Cosmochimica Acta 65, 1219–1231.
Olivier, N., Boyet, M., 2006. Rare earth and trace elements of microbialites in Upper Jurassic coral- and sponge-microbialite reefs. Chemical Geology 230, 105–123.
Parkinson, I.J., Pearce, J.A., 1998. Peridotites from the Izu–Bonin–Mariana forearc (ODP Leg 125): evidence for mantle melting and melt–mantle interaction in a supra-subduction zone setting. Journal of Petrology 39 (9), 1577–1618.
Paulick, H., Bach, W., Godard, M., Hoog, C.J., Suhr, G., Harvey, J., 2006. Geochemistry of abyssal peridotites (Mid-Atlantic Ridge, 15 20′N, ODP Leg 209): implications for fluid/rock interaction in slow spreading environments. Chemical Geology 234, 179–210.
Peacock, S.M., Wang, K., 1999. Seismic consequences of warm versus cool subduction metamorphism: examples from southwest and northeast Japan. Science 286, 937–939.
Pearce, N.J.G., Perkins, W.T., Westgate, J.A., Gorton, M.P., Jackson, S.E., Neal, C.R., Chenery, S.P., 1997. A compilation of new and published major and trace element data for NIST SRM 610 and NIST SRM 612 glass reference materials. Geostandards Newsletter — The journal of Geostandards and Geoanalysis 21 (1), 115–144.
Plank, T., Langmuir, C.H., 1998. The chemical composition of subducting sediments and its consequences for the crust and mantle. Chemical Geology 145, 325–394.
Rehkämper, M., Hofmann, A.W., 1997. Recycled ocean crust and sediment in Indian Ocean MORB. Earth and Planetary Science Letters 147, 93–106.
Rose, A.W., Hawkes, H.E., Webb, J.S., 1979. Geochemistry in Mineral Exploration (Second Edition). New York, Academic Press. 657 pp.
Russell, J., Chadwick, B., Krishna Rao, B., Vasudev, V.N., 1996. Whole-rock Pb/Pb isotopic ages of Late Archaean limestones, Karnataka, India. Precambrian Research 78, 261–272.
Ryan, J.G., Morris, J., Tera, F., Leeman, W.P., Tsvetkov, A., 1995. Cross-arc geochemical variations in the Kurile arc as a function of slab depth. Science 270 (5236), 625–627.
Salters, V.J.M., Stracke, A., 2004. Composition of the depleted mantle. Geochemistry Geophysics Geosystems 5 (5). doi:10.1029/2003GC000597.
Sato, H., 1977. Nickel content of basaltic magmas: identification of primary magmas and a measure of the degree of olivine fractionation. Lithos 10 (2), 113–120.
Savov, I.P., Ryan, J.G., D'Antonio, M., Fryer, P., 2007. Shallow slab fluid release across and along the Mariana arc-basin system: insights from geochemistry of serpentinized peridotites from the Mariana forearc. Journal of Geophysical Research 112. doi:10.1029/2006JB004749.
Savov, I.P., Ryan, J.G., D'Antonio, M., Kelley, K., Mattie, P., 2005a. Geochemistry of serpentinized peridotites from the Mariana Forearc Conical Seamount, ODP Leg 125: implications for the elemental recycling at subduction zones. Geochemistry Geophysics Geosystems 6 (4). doi:10.1029/2004GC000777.
Savov, I.P., Guggino, S, Ryan, J.G., Fryer, P., Mottl, M.J., 2005b. Geochemistry of serpentinite muds and metamorphic rocks from the Mariana forearc, ODP Sites 1200 and 778–779, South Chamorro and Conical Seamounts. In: Shinohara, M., Salisbury, M.H., Richter, C. (Eds.), Proceedings of the Ocean Drilling Program: Scientific Results, vol. 195, pp. 1–49.
Scambelluri, M., Müntener, O., Ottolini, L., Pettke, T.T., Vannucci, R., 2004. The fate of B, Cl and Li in the subducted oceanic mantle and in the antigorite breakdown fluids. Earth and Planetary Science Letters 222, 217–234.
Scambelluri, M., Bottazzi, P., Trommsdorff, V., Vannucci, R., Hermann, J., Gòmez-Pugnaire, M.T., Lòpez-Sànchez Vizcaìno, V., 2001a. Incompatible element-rich fluids released by antigorite breakdown in deeply subducted mantle. Earth and Planetary Science Letters 192, 457–470.
Scambelluri, M., Rampone, E., Piccardo, G.B., 2001b. Fluid and element cycling in subducted serpentinite: a trace-element study of the Erro-Tobbio high pressure ultramafites (Western Alps, NW Italy). Journal of Petrology 42 (1), 55–67.
Seyfried Jr., W.E., Chen, X., Chan, L.H., 1998. Trace element mobility and lithium isotope exchange during hydrothermal alteration of seafloor weathered basalt: an experimental study at 350 °C, 500 bars. Geochimica et Cosmochimica Acta 62, 949–960.
Seyfried Jr., W.E., Dibble Jr., W.E., 1980. Seawater–peridotite interaction at 300 °C and 500 bars: implications of the origin of oceanic serpentinites. Geochimica et Cosmochimica Acta 44, 309–321.
Shen, G.T., Dunbar, R.B., 1995. Environmental controls on uranium in reef corals. Geochimica et Cosmochimica Acta 59 (10), 2009–2024.
Smedley, P.L., Kinniburgh, D.G., 2002. A review of the source, behaviour and distribution of arsenic in natural waters. Applied Geochemistry 17, 517–568.
Soyer, W., Unworth, M., 2006. Deep electrical structure of the northern Cascadia (British Columbia, Canada), subduction zone: implications for the distribution of fluids. Geology 34, 53–56.
Stamoudi, C., 2002. Processus de serpentinisation des péridotites de Hess Deep et de la zone MARK. Unpublished PhD, Université Pierre et Marie Curie, Paris, 372 pp.
Sun, M., Kerrich, R., 1995. Rare earth element and high field strength element characteristics of whole rocks and mineral separates of ultramafic nodules in Cenozoic volcanic vents of southeastern British Columbia, Canada. Geochimica et Cosmochimica Acta 59 (23), 4863–4879.
Takahashi, Y., Minamikawa, R., Hattori, K.H., Kurishima, K., Nihou, N., Yuita, K., 2004. Arsenic behaviour in paddy fields during the cycle of flooded and non-flooded periods. Environmental Sciences Technology 38, 1038–1044.
Tenthorey, E., Hermann, J., 2004. Composition of fluids during serpentinite breakdown in subduction zones: evidence for limited boron mobility. Geology 32 (10), 865–868.
Thompson, G., Melson, W.G., 1970. Boron contents of serpentinites and metabaslts in the oceanic crust: implications for the boron cycle in the oceans. Earth and Planetary Sciences Letters 8, 61–65.
Turekian, K.K., Wedepohl, H., 1961. Distribution of the elements in some major units of the Earth's crust. Geological Society of America Bulletin 72, 175–192.
Ulmer, P., Trommsdorff, V., 1995. Serpentine stability to mantle depths and subduction-related magmatism. Science 268 (5212), 858–861.
Van Achterberg, E., Ryan, C.G., Jackson, S.E., Griffin, W., 2001. Data reduction software for LA-ICP-MS. In: Sylvester, P. (Ed.), Laser Ablation ICP-MS in the Earth Science. Mineralogical Association of Canada, pp. 239–243.
Vils, F., Pelletier, L., Kalt, A., Müntener, O., Ludwig, T., 2008. The lithium, boron and beryllium content of serpentinized peridotites from ODP Leg 209 (Sites 1272A and 1274A): implications for lithium and boron budgets of oceanic lithosphere. Geochimica et Cosmochimica Acta 72, 5475–5504.
Wang, J., Hattori, K.H., Stern, C.R., 2008. Metasomatic origin of garnet orthopyroxenites in the subcontinental lithospheric mantle underlying Pali Aike volcanic field, southern South America. Mineralogy and Petrology 94, 243–258.
Wei, W., Kastner, M., Dehyle, A., Spivack, A.J., 2005. Geochemical cycling of fluorine, chlorine, bromine, boron and implications for fluid–rock reactions in Mariana forearc, South Chamorro Seamount, ODP Leg 195. Proceedings of Ocean Drilling Program, Scientific Results 195, 1–23.
White, W.M., Albarède, F., Telouk, P., 2000. High-precision analysis of Pb isotope ratios by multi-collector ICP-MS. Chemical Geology 167, 257–270.
Wicks, F.J., Whittaker, E.J.W., 1977. Serpentine texture and serpentinization. Canadian Mineralogist 15, 459–488.
Wunder, B., Wirth, R., Gottschalk, M., 2001. Antigorite: pressure and temperature dependence of polysomatism and water content. European Journal of Mineralogy 13, 485–495.